Hydraulics Research
Wallingford

PERFORMANCE OF VORTEX INHIBITORS FOR RESERVOIR INTAKES

by

R W P May & I R Willoughby

Report SR 231
February 1990

Registered Office: Hydraulics Research Limited,
Wallingford, Oxfordshire OX10 8BA.
Telephone: 0491 35381. Telex: 848552

This report describes work funded by the Department of the Environment under Research Contract No PECD 7/6/113, Hydraulic Structures and Alluvial Processes. It is published on behalf of the Department of The Environment, but any opinions expressed in this report are not necessarily those of the funding Department. The work was carried out in the River Engineering Department of Hydraulics Research, Wallingford headed by Dr W R White. The nominated project officers were Dr R P Thorogood and Mr P Woodhead for DOE and Dr W R White for HR.

Performance of Vortex Inhibitors for Reservoir Intakes

R W P May
I R Willoughby

Report SR 231
February 1990

ABSTRACT

An experimental study, funded by the Department of the Environment, was made to determine the relative effiencies of a variety of vortex inhibitors suitable for horizontal intakes in reservoirs. The inhibitors were tested in two specially constructed tanks. The first measured 6m x 6m in plan and 3.6m in depth and was equipped with pumps having a combined capacity of $0.21m^3/s$. The second tank reproduced the geometry of the first one at a scale of about 1:3.2, and had dimensions of 1.83m x 1.83m in plan and 1.12m in depth with a maximum flow capacity of $0.024m^3/s$.

In each tank a set of base data was established using a plain intake that was prone to vortex action ; this was provided by a circular pipe projecting horizontally into the tank. Flow rates were determined corresponding to three stages of vortex development : (1) formation of surface dimple ; (2) draw of material to the intake by a water core ; and (3) formation of a continuous air core to the intake. The circulation strengths of the vortex motion were also measured photographically using floats. This set of data was obtained for three depths of submergence corresponding to 5.2D, 8.2D and 11.7D, where D is the internal diameter of the intake.

The inhibitors were tested by adding them to the plain intake and measuring the discharge at which each vortex strength occurred at each of the three submergence levels. Thirty configurations were studied including headwalls (vertical, sloping and set back), flow straighteners (fins and cruciforms), bar screens and floating rafts. The results were expressed in terms of discharge ratios relative to the base data obtained with the plain projecting pipe. A ranking procedure was then applied in order to group the inhibitors into three performance bands : good, average and poor.

The "good" category comprised only vertical or near-vertical headwalls extending to the water surface. The best design was a vertical full-height flush headwall which had an average discharge ratio of 2.6, ie the discharge at which a certain strength of vortex occurred with the inhibitor was about 2.6 times the corresponding discharge for the plain horizontal pipe. The "average" category covered discharge ratios from 2.0 to 1.5; the best two of these designs were a hooded bar screen and an extended longitudinal fin along the top of the horizontal pipe. Low-cost inhibitors with reasonable performance (discharge ratio of about 1.6) included a floating raft and a newly-developed hanging cord or chain. Adding fins to the hanging chain improved its performance considerably.

Pressure measurements in the intake pipe were made to determine the effect of vortex strength and inhibitor design on head losses. No measurable change in entrance loss due to increasing vortex strength was detected. The effect of intake configuration on entrance loss was also small and of the order of $\pm$ 5% ; the lowest loss coefficient occurred with the flush vertical headwall. The mean energy gradient along the intake pipe was well predicted by the Colebrook-White equation.

The relationship between vortex strength and discharge was studied in detail for two intake configurations : the plain horizontal pipe representing an "inefficient" design, and the pipe with an extended longitudinal fin representing an "efficient" one. It was found that the two intakes had different strength/discharge relationships even though the approach conditions of the flow were the same. The conclusion, therefore, is that the strength of vortex which develops at an intake is partly determined by its geometry and not solely by the approach conditions (as is sometimes supposed). Based on these findings, a general description of vortex action at intakes is presented in the report.

SYMBOLS

A	Effective cross-sectional area of intake
C	Coefficient of discharge
C_a	Effective contraction coefficient
D	Internal diameter of intake
d	Depth below water surface
F	Froude number
g	Acceleration due to gravity
H	Depth of water
h	Static head
h_c	Additional velocity head due to flow contraction
h_o	Total head
Δh	Head loss
h_i	Head loss at entrance to intake
i	Energy gradient
i_{cw}	Energy gradient predicted by Colebrook-White equation
K	Kolf number
k_i	Entrance loss coefficient
k_s	Hydraulic roughness in Colebrook-White formula
L	Length dimension
Q	Volumetric discharge
R_e	Reynolds number
R_r	Radial Reynolds number
r	Radius
r_o	Radius of rotational vortex core
S	Submergence measured to centreline of intake
S_c	Critical submergence for specified vortex strength
u	Velocity component in x-direction
V	Flow velocity
$\underset{\sim}{V}$	Velocity vector
v	Velocity component in y-direction
v_t	Radial velocity component
v_θ	Tangential velocity component
W	Weber number
w	Velocity component in z-direction
x	Distance along horizontal x-axis
y	Distance along horizontal y-axis
z	Distance along vertical z-axis
α	Energy coefficient for non-uniform velocity distribution
Γ	Circulation strength (Equation 3)
Γ_o	Circulation strength of vortex core
ζ	Vorticity component about vertical z-axis
θ	Angular position in cylindrical co-ordinates
ν	Kinematic viscosity of liquid
ρ	Density of liquid
σ	Surface tension of liquid

CONTENTS

CONTENTS (CONT'D)

1 INTRODUCTION

In the field of civil engineering hydraulics, vortices are most commonly encountered at intakes which draw water from tanks, reservoirs, rivers and the sea. Vortex formation is usually undesirable and may cause the following problems:

- additional head losses in the intake
- draw down of floating debris
- structural vibrations
- uneven running and reduced efficiency of hydraulic machinery due to swirl and entrained air
- slug flows in downstream conduit due to entrained air
- increased risk of cavitation

Much research has been carried out on vortices at intakes, and the principal aspects which have been studied are:

- mathematical descriptions of vortex motion
- experimental measurements of fluid motion near the vortex core
- determination of critical conditions for vortex formation using physical models
- scale effects in physical models

In the case of pumping stations, experience accumulated from model studies and prototype installations has helped to identify design features which will prevent or inhibit the formation of vortices. References such as Prosser (1977) therefore provide guidance on the necessary approach conditions, the geometry of the sump, the position of the suction pipe and the minimum depth of submergence.

In the case of reservoirs, less progress has been made. The mechanism by which vortices are generated is not properly understood, and mathematical solutions of the theoretical Navier-Stokes equations cannot at present be obtained for the complex geometries which exist in natural reservoirs. Experimental research has provided data on the critical conditions for vortex formation, but each study tends to be specific to the particular type of intake and reservoir geometry tested. Various criteria for scaling vortex motion between model and prototype have been proposed, but none is yet widely accepted, due partly to the difficulty of obtaining field data.

The experimental study described in this report was carried out at Hydraulics Research (HR) to compare the performance of different types of vortex inhibitor and to provide guidance on suitable designs for reservoir intakes. If small-scale tests show that inhibitor A is more effective than inhibitor B, then type A can also be expected to be superior at full size. The emphasis in this study on comparative performance therefore enabled the problem of scale effects to be partially side-stepped. Nevertheless, useful data on some of the more general aspects described above were also obtained in the course of the tests.

The HR study was commissioned by the Construction Industry Directorate of the Department of the Environment. The first stage of the work was completed in 1987 and was described in HR Report SR 122 (see Perkins (1987)). Fourteen types of intake design were studied in a specially constructed tank measuring 6m by 6m in plan and 3.6m in depth. Further tests were then made using a smaller tank which reproduced the geometry of the first one at a scale of approximately 1:3.2. Eighteen types of intake were studied in the second tank, some of these being equivalent to designs tested previously in the large one.

The second stage of the HR study was more limited in scope, and covered three recommendations for further work which were made after completion of the first stage. The tests were carried out in the smaller tank and investigated:

- the performance of some additional inhibitors
- the effect of vortex formation on pressures and head losses in selected intakes
- the effect of intake type on vortex strength

Section 2 of this report reviews the main factors which govern vortex motion, and puts forward an overall explanation of how vortices are formed in reservoirs. Section 3 briefly describes the tests which were carried out in the first stage, and for completeness repeats the experimental data and the main results; full details of this work can be found in Perkins (1987). The experimental procedure and the data obtained from the second stage of the project are described in Section 4, and all the results are analysed and discussed in Section 5.

2 VORTEX THEORY

2.1 Principles

The motion of an element of fluid can be decomposed into the following three parts (see Stokes (1845)):

- translation - movement from A to B

- distortion - change in shape due to convergence or divergence of flow

- rotation - spin about its own axis

All flows involve translational movement, and distortion must occur if they are two-dimensional or three-dimensional. Rotational motion, however, represents "wasted" energy and does not contribute to the overall flow : if a fluid element rotates once between A and B, it arrives in the same state as if it had not had any spin. In an "ideal" non-viscous fluid, the amount of rotation is arbitrary and can have any value including zero (eg liquid spinning inside a circular container). An "irrotational" motion, in which no fluid particles have any spin, represents the most energy-efficient solution to any flow problem. However, in a "real" viscous liquid, rotational motion is generated as a result of the "no-slip" condition which applies between fluid particles and an adjacent solid boundary. The amount of rotation is therefore no longer arbitrary, but determined by the effective viscosity of the fluid, the shape of the boundaries and the rate of flow.

The rotation of a fluid element is described in terms of its vorticity which is defined as being equal to twice its angular rate of rotation. Using rectangular co-ordinates (x, y, z) with corresponding velocity components (u, v, w), the vorticity component ζ about the z-axis is

$$\zeta = \frac{\partial v}{\partial x} - \frac{\partial u}{\partial y} \tag{1}$$

with equivalent results applying for the two other axes. In terms of polar co-ordinates (r, θ, z) and the corresponding velocity components (v_r, v_θ, w), ζ is given by

$$\zeta = \frac{1}{r}\left[v_\theta + r\,\frac{\partial v_\theta}{\partial r} - \frac{\partial v_r}{\partial \theta}\right] \tag{2}$$

It should be noted that the vorticity is a vector quantity.

The circulation Γ is defined as the line integral of the velocity vector $\underline{V}$ around a closed circuit C in the fluid, and in rectangular co-ordinates is given by

$$\Gamma = \oint_C (u\,dx + v\,dy + w\,d\,z) \tag{3}$$

The corresponding result in polar co-ordinates is

$$\Gamma = \oint_C (v_r\,dr + r\,v_\theta\,d\theta + w\,d\,z) \tag{4}$$

It can be seen from the definition of Γ that it is a scalar quantity and not a vector like vorticity.

From Stokes' theorem it can be shown that, if for example the circuit C lies in the x,y plane, then

$$\Gamma = \int_A \zeta\,dx\,dy \tag{5}$$

where A is the area enclosed by C. The circulation Γ therefore provides a measure of the amount of vorticity contained within the area A, and can be evaluated by measuring the velocity around a suitable closed circuit.

Experimental measurements of fluid motion around a well-established vortex show that practically all the vorticity is concentrated close to the core of the vortex, and that further away the flow is effectively irrotational. A simplified but useful model of such a motion is provided by the two-dimensional Rankine vortex. Within a radius of $r = r_o$, the fluid is assumed to be rotating as a solid body with an angular velocity ω. The flow within this core is therefore rotational with uniform vorticity of $\zeta = 2\omega$, see Equation (2). The value of circulation for a circuit of radius $r = r_o$ just enclosing the core is found from Equation (5) to be

$$\Gamma_o = 2\pi r_o^2 \omega \tag{6}$$

The flow outside the core is assumed to be irrotational and have no vorticity. In this region, the value of circulation for any circuit which does not enclose the core is $\Gamma = 0$. However, for any circuit which fully encloses the core, the circulation will be constant and equal to Γ_o above. From Equation (4) it follows that the tangential velocity v_θ at radius r is given by

$$v_\theta = \frac{\Gamma_o}{2\pi r}, \text{ for } r \geq r_o \tag{7}$$

The strength of such a vortex can therefore be determined by measuring tangential velocities outside the core.

The Rankine model assumes that the motion is purely rotational, and does not take account of the three-dimensional nature of the flow and its convergence towards the intake. A more realistic model for flow towards a vertical intake was developed by Sanmuganathan (1986). This combined a vertical Rankine vortex with a three-dimensional potential sink having a uniform distribution of strength over the face of the intake. The model provides a helpful description of the conditions necessary for the development of an air-entraining vortex. Near the surface, rotation of the fluid lowers the pressure below atmospheric and allows air to penetrate part-way into the vortex core. Near the intake, the convergence of the flow also produces sub-atmospheric pressures in its vicinity. However, at intermediate depths, the fluid pressure may still be above atmospheric and therefore acts as a barrier to the penetration of the air core. The intake will begin to entrain air when the circulation strength and/or the discharge rate are sufficient to produce sub-atmospheric pressures in the fluid at all points on the vertical centreline of the intake.

The strength of a vortex can be judged qualitatively by the appearance of certain features. Figure 1 shows the method of classification adopted for the present study, whereby strength 1 corresponds to the start of surface rotation and strength 6 to a continuous air core to the intake. The limiting flow conditions associated with the appearance of a given type of vortex are often expressed in terms of the critical submergence S_c; for a given flow rate and circulation strength, S_c is the maximum depth of fluid above the intake at which that vortex type will occur. Alternatively, for a given submergence and circulation strength, the limit may be defined in terms of the corresponding minimum flow rate Q_c.

2.2 Governing factors

Results of vortex studies are often presented in non-dimensional form, but previous investigators have grouped the parameters in a variety of ways. The following is a brief summary of some of these groupings.

1. Geometric parameters The dimensions of the tank and the position of the intake may be related to the size of the intake (diameter D if circular), the depth of water H in the tank, or the submergence S of the centre of area of the intake.

2. Reynolds number (ratio of inertial to viscous forces)

$$R_e = \frac{Q}{L\nu} \text{ or } \frac{VL}{\nu} \tag{8}$$

where Q is the flow entering the intake, V the average velocity at the intake and L a dimension of the intake (eg the diameter D). Alternatives are

$$R_r = \frac{Q}{S\nu} \text{ or } \frac{VS}{\nu} \tag{9}$$

which are termed radial Reynolds numbers by Anwar (1966).

3. Froude number (ratio of inertial to gravitational forces)

$$F = \frac{Q}{(gL^5)^{1/2}} \text{ or } \frac{V}{(gL)^{1/2}} \quad (10)$$

An alternative type of Froude number is given by what is sometimes termed the coefficient of discharge

$$C = \frac{Q}{A(2gS)^{1/2}} \quad (11)$$

where A is the effective area of the intake.

4. Weber number (ratio of inertial to surface tension forces)

$$W = V \left(\frac{\rho L}{\sigma}\right)^{1/2} \text{ or } V\left(\frac{\rho S}{\sigma}\right)^{1/2} \quad (12)$$

where σ is the surface tension and ρ the density of the liquid.

5. Kolf number (ratio of centrifugal to inertial forces)

$$K = \frac{\Gamma}{VL}, \frac{\Gamma L}{Q} \text{ or } \frac{\Gamma}{L(2gS)^{1/2}} \quad (13)$$

where Γ is the circulation defined by Equation (3)

Many studies are concerned with identifying the critical flow conditions (submergence S_c or discharge Q_c) at which a given strength of vortex first occurs : eg surface dimple, material drawdown or continuous air core (see Figure 1). A quantity such as S_c/L is normally assumed to be a dependent parameter, but it is less easy to categorise some of the dimensionless numbers described above. If the circulation Γ is forced by jets or vanes, the Kolf number K is an independent parameter; in a reservoir, Γ is determined by the geometry and the fluid properties so that K is a dependent parameter. The quantity C in equation (11) only becomes a true discharge coefficient when applied to an orifice that discharges directly to atmosphere; C is then a dependent variable since Q and S are directly related. However, if there is a pipeline or pump downstream of the intake, Q and S can usually be varied independently : C then loses its significance as a discharge coefficient and only represents an alternative and arbitrary type of Froude number.

2.3 Mechanisms of vortex formation

Although the basic principles of vortex motion are well established, it is still difficult to understand how vortices are generated at intakes and why they vary in strength and position in an unpredictable way. Partly, this is because classical fluid mechanics tends to deal with idealised situations in which irrotational and inviscid flows occur around concentrated regions of vorticity. The behaviour of viscous fluids can be described by the Navier-Stokes equations, but to obtain valid solutions for realistic reservoir shapes it appears necessary to develop improved computational techniques and a better understanding of factors such as turbulence and eddy viscosity (see, for example, the discussion by Hecker in Knauss (1987), pp33-38).

In pumping stations, it is clear that vortices can result from flow separation at obstructions and discontinuties and from flow along vertical side walls. In reservoirs, it is harder to see where the vorticity comes from when the lateral boundaries are very far removed from the intake. The following is an attempt to provide a qualitative description of the phenomenon which can be of use when considering experimental results and the problems of scaling.

Consider first the simplified case of a large semi-infinite reservoir which is rectangular in plan. If the approaching flow is distributed uniformly across the width of the reservoir and the intake is centrally located near the closed end, there will be no net generation of vertical vorticity at the sides; flux of positive vorticity along one side will be balanced by an equal flux of negative vorticity along the other. However, all the water possesses "background" vorticity due to the earth's rotation and in the absence of other sources this can produce a vortex at the intake. As the flow converges towards the intake, it carries vertical vorticity with it; vorticity is also removed from the reservoir by swirling flow entering the intake. The vortex at the intake will become stronger until there is a balance between the amount of vorticity entering and leaving the core; note that the strength is not determined directly by the magnitude of the vorticity flux but by the difference between the rates of inflow and outflow. If the vortex is produced by the earth's rotation (the Coriolis effect), it will always rotate anti-clockwise in the northern hemisphere (when viewed from above).

Although the Coriolis effect always provides a source of net vorticity (except on the equator), it appears to be too weak to account for the vortices which readily occur in small tanks and models of reservoirs; the sense of rotation of these vortices often varies with time and the depth of flow. Natural reservoirs are never symmetrical, and many researchers suggest that the vortices are the direct result of the intake being off-centre or the approach conditions being non-uniform. However, if the fluid were inviscid, it would always be possible to identify an irrotational solution to the flow problem (from Laplace's equation) which did not require any vortex or circulation at the intake. Methods which attempt to determine the circulation strength from the curvature of the approach flow are therefore invalid. Instead, the source of the vorticity can be understood in terms of modifications to the irrotational flow pattern caused by bed friction and fluid viscosity. Curvature arising from the irrotational motion will produce horizontal velocity gradients, but these will be reduced by frictional and viscous effects; vorticity will therefore be generated between the vertical shear layers and carried by the flow towards the intake. However, as the circulation strength increases at the intake, it also begins to alter the pattern of the approaching flow, and this modifies the intensity of the vorticity which is generated throughout the reservoir. The time lag between changes in the flow pattern and the arrival of the convected vorticity at the intake serves to explain why weak vortices seldom appear to be stable : the flow field never reaches an equilibrium state but is continuously evolving.

This description also sheds light on the role of vortex inhibitors. These usually act to reduce the curvature of the flow around an intake and promote more uniform approach conditions. An inhibitor therefore influences the general flow pattern in a reservoir and hence the amount of vorticity produced. The circulation strength which appears at an intake is therefore not fixed solely by the reservoir shape but is also affected by the design of the intake. The development of an air core within a vortex depends primarily on the circulation strength and the flow rate entering the intake, as demonstrated by the theoretical model developed by Sanmuganathan (1984). The inhibitor should therefore be seen not as making it harder for a vortex of given strength to produce an air core but as reducing the strength of the vortex generated by the flow in the reservoir.

Several conclusions can be drawn from this discussion of vortex generation.

(1) The circulation strength of a vortex is not determined directly by the shape of a reservoir but by modifications to the irrotational flow pattern caused by frictional effects.

(2) The strength of a vortex is determined by the balance between fluxes of vorticity approaching and leaving the intake.

(3) The establishment of a vortex alters the flow field and the amount of vorticity generated in the reservoir.

(4) The strength of a vortex is influenced by the design of the intake as well as by the geometry of the reservoir.

(5) The effects of fluid viscosity and bed roughness need to be reproduced correctly in a reservoir model if it is to predict correctly the circulation strength at an intake.

3 STAGE ONE TESTS

3.1 Large tank

A tank measuring 6m x 6m in plan and 3.6m in depth was constructed from bolted steel panels and supported on 0.8m high concrete piers (see Figure 2 and Plate 1). The area beneath and around the tank was enclosed to form a sump measuring 8.85m x 8.85m.

The facility was equipped with two pumps having capacities of $0.14m^3/s$ and $0.07m^3/s$ and supplying a common 225mm diameter inlet manifold inside the tank. Two full-height screens containing hairlok were used to still the flow entering the test area of the tank and produce a uniform distribution across its width. The outlet from the tank was provided by a 225mm diameter pipe located low down in the wall immediately opposite to the inlet manifold.

The pipework was designed so that tests could be made either with the outlet from the tank connected directly to the pumps ("closed" system) or with the outlet discharging under gravity into the sump beneath the tank ("open" system), see Figure 2. Recirculating the water directly from the tank outlet to the inlet manifold, using the first option, was suitable when carrying out tests at fixed water levels. The tank was filled to the required depth, and the flows from the pumps were adjusted by means of gate valves in the delivery pipes; British Standard orifice plates were used to measure the flow rates. The second option allowed tests to be carried out with the tank emptying under gravity (like a bath-tub) with the discharge rate and the water level varying continuously with time; the head loss between the outlet pipe and the sump could be altered by means of control valves.

A working platform was provided at the top of the tank along two of its sides. It was also necessary to be able to make measurements and observations near the centre of the tank and over the full range of water levels. A movable scissors-type platform was therefore constructed, as shown in Plate 2. The platform could be winched along a supporting beam, which in turn was mounted on two rails on opposite sides of the tank. The scissors design allowed the platform to be adjusted to any level between the top water level and the floor of the tank.

The effective working area of the tank measured 4.57m long x 6.0m wide, and alternative designs of intakes and inhibitors were tested by connecting them to the 225mm diameter outlet pipe (see Figure 2). As explained in Section 1, the performance of the inhibitors was to be evaluated by comparing them with a basic type of intake which was prone to vortex formation. Initial tests showed that no significant vortex action occurred with a flush intake and uniform approach conditions. In order to establish a suitable base condition, it proved necessary to use a 198mm diameter pipe projecting horizontally into the tank and to make the approach conditions asymmetrical. The latter was achieved by attaching plastic sheeting to the inner hairlok screen so as to block off completely the right-hand half of the screen (viewed from the outlet pipe) over the full depth of the tank. It then proved possible with this arrangement to produce stable vortices with well-defined air cores extending from the water surface to the intake (see Plate 3).

Tests with this basic configuration were carried out with three different water depths in the tank, namely 1.2m, 1.8m and 2.5m; note that the centre-line of the intake was located 0.175m above the floor of the tank. The water was re-circulated by the pumps as a "closed" system, and the flow rate increased in steps to produce different stages of vortex development. At each water depth, values of flow rate Q and circulation strength Γ (see 2.1) were measured corresponding to three of the vortex types shown in Figure 1:

- surface dimple - strength 2
- draw-down of small pieces of polystyrene - strength 4
- continuous air core to intake - strength 6

The values of circulation were determined from time-exposure photographs of small surface floats circulating around the vortex core.

Having established this base data for the plain projecting pipe, similar tests were carried out with each of the vortex inhibitors shown in Figure 3. The reasons for the choice of the different types of inhibitor were as follows.

(1) Headwall

The preliminary tests in the large tank showed that a vertical wall flush with the end of the intake was efficient in preventing vortex formation. The relation between size of headwall and reduction in vortex strength was therefore investigated using four heights of headwall (related to the standard water depths of 1.2m, 1.8m and 2.5m used in the tests).

(2) Longitudinal fin

Observation of the flow patterns around the plain projecting pipe showed that a spiral motion was induced by water flowing across the line of the pipe before turning downwards and back towards the inlet. A longitudinal fin was therefore added along the top of the pipe with the objective of straightening the flow by reducing the initial transverse motion. The effect of varying the height of the fin and projecting it forward was investigated in four separate tests.

(3) Cruciform

Straightening the flow as it enters the pipe might be expected to reduce the strength of any spiral motion leading to vortex formation. Four vanes forming a cruciform were therefore inserted in the end of the pipe. Tests were made to study the effect of extending the vanes forward and of rotating them by 45° to the diagonal position.

(4) Roughness board

Earlier work by Anwar (1968) showed that roughening the floor of the tank around a vertical intake reduced the strength of the vortex motion. A test was therefore made with 36 cubes arranged horizontally in front of the intake to increase the amount of energy dissipation.

(5) Square intake

The effect of cross-sectional shape was investigated by testing a square intake having the same cross-sectional area as the 198mm diameter pipe.

It should be pointed out that the experiments described above were not easy to carry out but required long, careful observations. The strength and position of the vortices tended to vary in an apparently random fashion, and in some cases they would disappear completely for long periods of time. The results were, therefore necessarily somewhat objective, and it was not always possible to achieve good repeatability. In most tests, a single surface vortex formed above the intake (rotating anti-clockwise when viewed from above), but occasionally a second weaker vortex would circulate around the primary vortex and sometimes disrupt and cause it to break up. The development of unseen secondary vortices may be the reason why visible vortices suddenly weaken and disappear.

3.2 Small tank

The tests described in Section 3.1 proved to be very time-consuming, and it was decided that results could be achieved more rapidly using a smaller rig. A tank measuring 1.83m x 1.83m in plan and 1.12m in depth was available and had the advantage that two of its sides were of perspex. The tank was therefore fitted with an inlet manifold and baffle screen so as to provide the same geometrical shape as the large tank (see Figure 4). The rig was operated as a "closed" system with the flow recirculated by a pump with a capacity of $0.026m^3/s$. The horizontal intake projecting into the tank was represented by a 0.50m long pipe with an internal diameter of 63mm and installed so that its centre-line was 55.5mm above the floor of the tank.

Based on plan dimensions, the scale ratio between the small and large tanks was 1:3.28. Based on intake diameters, the scale ratio was 1:3.14; this figure was used when determining the water depths used in the tests. Relatively larger flow rates could be achieved in the small tank; the ratio of the two pumping capacities was 1:8.75 whereas the value required for Froudian similarity was only 1:17.9.

Tests were carried out in a similar way to those in the larger tank, using three water depths of 0.382m, 0.573m and 0.795m. As before, the flow rates corresponding to the onset of vortex types 2, 4 and 6 in Figure 1 were recorded, and photographs of float tracks taken in order to determine the circulation strength Γ (see Plates 4 and 5).

The plain projecting pipe was tested first in order to establish a set of base data against which the inhibitors could be compared. It was found that air-entraining vortices could be produced with the flow from the manifold entering uniformly across the full-width of the tank. This contrasted with experiences in the large tank where it had proved necessary to blank off half the width of the baffle screen in order to produce significant vortex motion. This arrangement was also studied in the small tank but it was found that strong asymmetric flow across the line of the intake disrupted the vortices and prevented them becoming established. The reason for this difference in flow behaviour for the two tanks was not clearly identified but might have been the relatively higher flow rates used in the small tank. Since the inhibitors were being tested on a comparative basis, it was considered that a change in the inlet arrangements would not invalidate conclusions about their relative efficiencies.

The types of inhibitor which were studied in the small tank are shown in Figure 5. Some of these designs were similar to some of the ones tested in the large tank but others represented new arrangements. Brief descriptions of the inhibitors in Figure 5 are now given.

(1) Vertical headwall

The headwall was made relatively wider than those tested in the large tank, because in the latter it had been found that flow separation at the ends of the wall could give rise to additional vortices. In the small tank, the headwall extended above the maximum water level used. The effect of projecting the end of the intake slightly beyond the wall was investigated, and in one case a fin of height D was added to the top of the projecting pipe.

(2) Sloping headwalls

The 80° slope represents the type of arrangement that can occur at an intake in the upstream face of a concrete dam. The 1:3 in slope is more typical of the arrangement for an embankment dam. The 80° headwall extended above the maximum water level ; the 1:3 slope headwall extended back to the vertical side of the tank and was submerged at all three water levels used in the tests.

(3) Longitudinal fin

These tests repeated three of the configurations studied in the large tank (see Figure 3).

(4) Cruciform

This test repeated one of the configurations studied in the large tank (see Figure 3).

(5) Floating raft

Rafts moored above intakes have been used in some reservoirs (eg Kariba). Two sizes of square raft (made from thin wooden strips separated by gaps of equal width) were tested. The length of the mooring line from the raft to the soffit of the intake allowed it to move within a 45° cone. A keel (see dimension k in Figure 5) was added to the larger raft in order to help it remain longer at the centre of the vortex. Spinning of the raft tended to tangle the mooring line, and this sometimes prevented it following the movement of the vortex.

(6) Individual fins

Short fins staggered along the line of the pipe were studied to see if they would be more effective than a solid fin (see (3) above) at disrupting the transverse flow over the pipe.

(7) Submerged screen

A bar screen similar in size and construction to the smaller raft was fixed slightly above the soffit of the intake. This location was chosen so that the screen could disrupt any vortex core entering the intake without significantly increasing the head loss.

(8) Hanging cord

This was suggested by the tests with the moored raft, and is illustrated in Figure 6. The top of the cord was fixed above the water surface and behind the face of the intake where the vortices tended to form. The bottom of the cord just reached to the soffit of the intake and was weighted. Although only brief exploratory tests were carried out with this design, they were sufficient to indicate its effectiveness. When a vortex developed over the intake, the cord tended to be drawn towards the core, thereby disrupting its growth. The cord was not subject to the tangling problem experienced with the mooring line for the floating raft.

3.3 Results

Table 1 gives the results which were obtained with the inhibitors in the large tank. The threshold conditions for each inhibitor are listed for three different vortex strengths at each of the three different water levels. The type of vortex was classified by observation using the strength scale in Figure 1. Measurements of circulation strength and discharge entering the intake were made for the threshold conditions corresponding to dimple formation (strength 2), material draw-down (strength 4) and continuous air core (strength 6). Values of circulation were calculated from float tracks using Equation (7); each value in the Table represents the mean of about 10 to 15 measurements. The maximum pumping capacity of $0.205m^3/s$ was not sufficient to produce strong vorticies with some of the inhibitors; these cases are indicated in Table 1 by a threshold discharge $> 0.205m^3/s$.

The corresponding set of results for the inhibitors in the small tank is contained in Table 2. A value of threshold discharge > $0.0263 m^3/s$ indicates that the pumping capacity was insufficient to produce that particular strength of vortex.

The direction of primary vortex rotation in the large tank was always anti-clockwise (viewed from above), which was consistent with the asymmetric approach conditions imposed on the flow. In the small tank, where the approach conditions were uniform, the primary vortices generally rotated anti-clockwise. However, in four tests (out of a total of about 130) stable clockwise vortices occurred with strengths similar to those of the usual anti-clockwise ones. As mentioned in 3.1, weaker secondary vortices also tended to form at the surface, and these often had a clockwise rotation.

4 STAGE TWO TESTS

4.1 Additional inhibitors

Further tests on the relative efficiencies of inhibitors were carried out in the small tank to extend the range of the previous work. The additional inhibitors are shown in Figure 6, and the reasons for their choice were as follows:

(1) <u>Square intake</u>

The cross-sectional area of the intake was made equal to that of the 63mm diameter pipe used in the other tests. This type was included so that a comparison could be made with the square intake tested in the large tank.

(2) Hooded screen

The Stage 1 tests with the submerged bar screen had shown that the vortex core tended to avoid the screen by entering the intake from the side. The bars were therefore extended downwards around the sides (but not the front) of the horizontal screen to prevent this happening.

(3) Hanging cord

More extensive tests were carried out with the plain cord, which had been studied briefly in Stage 1 (see 3.2). A series of fins was then attached to the cord so as to make it easier for the cord to be drawn towards the centre of any developing vortex.

The square intake, the hooded screen and the plain cord were tested in the same way as the previous designs of inhibitor (see 3.2). The threshold values of discharge and circulation strength corresponding to the three stages of vortex development are listed in Table 3 for each of the three water levels used earlier.

The standard comparative technique did not prove appropriate for the hanging cord with the fins because it tended to break up the vortex before a full set of measurements could be taken. Its performance was therefore judged by comparing the percentage of time that a certain strength of vortex occurred at the pipe intake with and without the hanging cord. The tests were carried out in the small tank using the three standard depths and a range of discharges; each test was continued for one hour. The relative durations of the difference strengths of vortex are summarised in Table 4.

4.2 Head losses at intakes

The effect of vortex motion on the head loss at an intake was investigated by measuring pressures along the 63mm diameter intake pipe in the small tank. Four sets of pressure tappings were installed along the side and invert of the pipe as shown in Figure 7. Tests were carried out at water levels of 0.382m, 0.573m and 0.795m using the following intake configurations, all but one of which had been studied in the previous tests:

(1) plain projecting pipe (Figure 4);
(2) vertical headwall (Figure 5);
(3) hooded screen (Figure 6);
(4) vertical headwall and hooded screen (new combination).

Pressure measurements in the intake pipe were made over a range of discharges for each configuration and water level. The maximum flow rate that could be used in these tests was only about 50% of the available pump capacity; higher discharges produced pressures that were too low to be measured by the available manometer system. Due to this limitation, it was not always possible to produce such strong vortex action as had been observed in the earlier tests.

Representative plots of the pressure measurements are shown in Figures 8 and 9 for the case of the hooded screen. Assume that the overall water depth in the tank is H and that a pressure tapping in the pipe is located z above the floor. If the pressure at the tapping causes the water level in the manometer to fall a distance d below the water surface in the tank, then the static pressure head at the tapping is

$$h = H - z - d \tag{14}$$

If the velocity distribution in the pipe is assumed to be uniform, the total head h_o relative to the floor of the tank is given by

$$h_o = h + z + \frac{V^2}{2g} \tag{15}$$

where V is the mean velocity. The loss in total head Δh at the tapping is

$$\Delta h = H - h_o \tag{16}$$

which from Equations (14) and (15) can be shown to be equal to

$$\Delta h = d - \frac{V^2}{2g} \tag{17}$$

Values of Δh calculated from Equation (17) are plotted in Figures 8 and 9. Two points in particular should be noted. Firstly, the readings from the set of tappings close to the mouth of the intake lie well above the best-fit lines through the points given by the other tappings. This is to be expected because the local contraction of the flow entering the intake produces higher velocities and hence lower pressures than occur further downstream along the pipe. Secondly, the pressures and head-loss gradients given by the tappings along the side of the pipe (Figure 8) are different from those given by the tappings along the invert (Figure 9). This indicates that the velocity distribution in the pipe is not radially symmetric at each cross-section; this is not surprising given that the inlet conditions are not symmetrical and that any vortex from the surface tends to enter the pipe near the crown. Therefore, the velocity head term ($V^2/2g$) in Equation (17) should correctly be multiplied by an energy coefficient α (greater than unity). In practice values of α are difficult to measure or predict in such situations, and the experimental results are easier to use if they are analysed assuming a value of $\alpha = 1.0$.

The best-fit values of energy gradient i along the pipe were determined from the measurements of Δh, but omitting those given by the first set of tappings (for the reason explained above). Separate values of gradient for the side and bottom tappings are given in Table 5 for each test condition. Also included for comparison are values of i predicted by the Colebrook-White equation assuming a roughness of k_s = 0.003mm. It can be seen that in nearly all cases the energy gradients obtained from the bottom tappings were significantly larger than those given by the side tappings; the two gradients often differ by a factor of between 3 and 5. Given these very large differences, it is perhaps surprising to note how closely the mean values of the side and bottom gradients are predicted by the Colebrook-White equation (see Table 5).

The head loss Δh_i associated with an intake can be estimated by extrapolating the best-fit energy gradient back to the upstream end of the pipe. The corresponding values of the non-dimensional loss coefficient

$$k_i = \frac{\Delta h_i}{(V^2/2g)} \tag{18}$$

are listed in Table 5. Despite the large differences between the energy gradients given by the side and bottom tappings, the resulting values of k_i agree quite closely. The effects of intake geometry and vortex strength on k_i are discussed in Section 5.3.

As has been seen, the pressure measurements obtained from the most upstream set of tappings were affected by the local contraction of the flow entering the pipe. If the measured static pressure is h_c below the best-fit energy grade line, the effective contraction coefficient C_a for the cross-sectional area of the flow can be calculated from

$$C_a = [1 + \frac{h_c}{(V^2/2g)}]^{-\frac{1}{2}} \tag{19}$$

Mean values of C_a obtained from the side and bottom tappings are listed in Table 5.

4.3 Influence of intake geometry on vortex strength

The description of vortex formation put forward in Section 2.3 suggests that the circulation strength of a vortex depends on the local geometry of the intake as well as on the approach conditions and the flow rate. This hypothesis was tested by studying in detail the performance of two types of intake :

(1) <u>plain projecting circular pipe</u> - Figure 4 - representing an "inefficient" design prone to vortex action ;

(2) <u>extended longitudinal fin 2D high</u> - Figure 5 - representing one of the most effective designs of inhibitor.

Tests were carried out in the small tank with the standard water depths of 0.382m, 0.573m, and 0.795m. The flow rate was increased in steps up to the maximum available, and at each step the circulation strength of the vortex motion was determined photographically by means of float tracks. This procedure was used to establish the relationships between discharge and circulation strength for each water depth and type of intake. If two intakes experiencing the same approach conditions demonstrate different relationships, then it is reasonable to conclude that the local geometry of the intake affects the development of the vortex motion.

The measured discharges and circulations for the plain pipe and for the pipe with the longitudinal fin are listed in Table 6 and plotted in Figures 11 a, b and c (with the exception of two anomalous points for the fin at the lowest water level). As expected, the circulations which occurred with the longitudinal fin were generally lower than those observed with the plain pipe. These results are considered in more detail in Section 5.

5 ANALYSIS

5.1 Performance of Inhibitors

The relative performance of the different inhibitors can be judged by comparing their threshold discharges given in Tables 1, 2 and 3. Tables 7 and 8 give values of the discharge ratio obtained by dividing the threshold dicharges for a given water level and vortex strength by the corresponding discharge for the plain projecting pipe ; the larger the ratio, the more effective the inhibitor is at preventing vortex formation.

The available pumping capacity was not suffient in many of the tests to produce strong vortices ; a > sign in Tables 7 and 8 indicates that the particular vortex strength was not reached at the maximum flow rate. Some designs of inhibitor were tested in both the large and the small tanks, and it is interesting to compare the corresponding discharge ratios. Each value given below represents, for each vortex strength, the average of the ratios obtained with the three water levels used in the tests ; a > sign indicates that it was not possible to generate the particular vortex strength at all three levels.

Inhibitor Type	Average discharge ratios					
	Dimple		Material draw-down		Air-core	
	large tank	small tank	large tank	small tank	large tank	small tank
Fin, height D	1.41	1.35	1.01	1.24	>1.06	1.17
Fin, height 2D	>2.98	1.89	>1.67	>1.44	>1.26	>1.20
Extended fin, height 2D	>2.33	2.09	>1.92	>1.61	>1.53	>1.32
Cruciform, vertical	1.89	1.50	1.09	>1.69	>0.90	>1.25
Square inlet	1.27	1.37	>1.42	1.37	>1.00	1.11
Max values	>5.52	>6.26	>2.54	>2.02	>1.53	>1.46

The numbers along the bottom line give the value of the ratio which would occur if the maximum pumping capacity were insufficient to produce the given vortex strength at all three water levels. The lack of precise data for all vortex strengths makes it difficult to draw firm conclusions, but overall there is reasonable agreement between the results obtained in the large and small tanks : an inhibitor which performed well in the large tank (eg the extended fin) also performed well in the small one. Where it was not possible to produce a given vortex strength at the two higher water levels, the relative ranking of two inhibitors will depend only on the measurements obtained at the lowest level; experimental scatter can thus sometimes produce anomalous results (eg the cruciform which performed relatively better in the small tank).

In order to compare the performance of all the inhibitors that were tested, the following ranking procedure was applied. First, the average discharge ratio for each inhibitor and vortex strength was calculated using the measurements at the three different water levels (as described above). Next, the values for a given vortex strength were ranked by giving a score of 1 to the most effective inhibitor (with the highest average discharge ratio), 2 to the next and so on down the list. The scores for the vortex strengths corresponding to dimple formation and material draw-down were then weighted and added together. The weighting scale adopted was 2 for the material draw-down result and 1 for the dimple result, since the material draw-down limit is closer to the conditions at which problems might occur at an intake. Thus, if N inhibitors were tested and one design was the most effective at both stages of vortex development, then it would have been given a weighted score of $2x1 + 1x1 = 3$; similarly a design which was the least effective at both stages would have received a score of 3N. This ranking procedure was carried out separately for the tests in the large tank and the small tank, and the resulting percentage scores are shown in Tables 7 and 8.

Although the data for air-core formation would obviously have been relevant to the rankings, their inclusion was found to distort the results. This problem arose because the limits on pumping capacity prevented air cores from being generated with many of the inhibitors. As a result, these designs would have been ranked as first equal for air-core formation, even though some were considered to be more efficient than others. Concentrating on the data for the dimple stage (strength 2 in Figure 1) and the material draw-down stage (strength 4) was found to give results which were nevertheless consistent with those observed in the air-core tests. Hecker (1981) considered that the occurrence in a model of a continuous dye core between the surface and the intake (strength 3) was a suitable indicator of possible air-entrainment problems in the prototype.

Comparison of the scores in Tables 7 and 8 shows that the designs of inhibitor which were tested in both the large and small tanks generally appear in the same relative order in both lists. The full-height headwall was the most effective type and the plain projecting pipe was the least effective. It therefore proved possible to combine the two lists and produce the following ranking for all the inhibitors tested in this study (see Figures 3, 5 and 6). The only major anomaly occurred with the flush cruciform which performed better in the small tank than in the large one ; its overall ranking therefore reflects an average of the two sets of results.

GOOD (2.6 ≥ mean discharge ratio > 2.0)

1 Vertical flush headwall (full height, 12.3D)
2 Vertical headwall, pipe projecting 1.6D plus fin height D
3 Vertical headwall, pipe projecting 1.6D
4 80° flush headwall
5 Vertical headwall, pipe projecting 3.2D
6 80° headwall, pipe projecting 1.6D
7 80° headwall, pipe projecting 3.2D
8 Vertical headwall, pipe projecting 4.8D

*Note all these headwalls projected above the maximum water level studied in the tests

AVERAGE (2.0 ≥ mean discharge ratio > 1.5)

9 Hooded screen
10 Extended fin height 2D along pipe
11 1:3 slope headwall
12 Individual fins height 2D along pipe
13 Floating raft 3D/2 square
14 Hanging cord (no fins)
15 Floating raft D square
16 Flush fin height 2D along pipe
17 Floating raft 3D/2 square with keel

POOR (1.5 ≥ mean discharge ratio ≥ 1.0)

18 Flush cruciform in pipe
19 Submerged screen D square above intake
20 Square intake
21 Vertical flush headwall height 9.2D
22 Extended fin height D along pipe
23 Extended cruciform in pipe
24 Vertical flush headwall height 6.2D
25 Diagonal cruciform
26 Vertical flush headwall height 3.1D

27 Roughness board below pipe entrance

28 Flush fin height D along pipe

29 Plain projecting pipe (discharge ratio = 1.0)

The inhibitors have been divided into three broad categories and are arranged in order of decreasing efficiency within each category. As will be appreciated from the description of the ranking procedure, too much significance should not be attached to small differences of position in the list.

The results clearly demontrate that vertical or near vertical headwalls extending above the maximum water level were the most effective types of inhibitor tested in the study. Observations with the plain projecting pipe showed that the vortices usually formed in the region between the face of the intake and the back wall of the tank. A headwall therefore forces the vortex forwards and straightens the flow entering the pipe ; the presence of the wall also reduces the strength of a developing vortex by means of viscous dissipation.

Although a headwall may be the most efficient configuration, it is often not feasible to construct one at an intake located well away from the sides of a reservoir. If the headwall does not extend up to the water surface, then its performance is greatly reduced; the vertical headwalls with heights of 3.1D, 6.2D and 9.2D all came in the "poor" category when tested in water depths of up to 12.3D. In such cases it is better to use a structure around the intake that straightens the flow and makes it difficult for the vortex core to enter the intake. The hooded bar screen (no 9) was the most effective of these smaller structures ; the front face of the intake was left open but the bars above the intake and around the sides helped disrupt any vortex passing between them. The importance of the screens at the side is shown by the relatively poor performance of the submerged screen (no 19). A longitudinal fin 2D high mounted on top of the pipe and extending a distance 2D forward (no 10) proved similarly effective. This helped to prevent the establishment over the pipe of a strong spiral flow which was observed to be associated with the formation of a surface vortex.

The floating raft measuring 3D/2 square (no 13) and the plain hanging cord (no 14) were reasonably good, and either would provide a low-cost remedial solution for an existing intake suffering from vortex action. Problems were encountered in the model tests of the raft as its mooring line became badly tangled by the spinning of the raft ; a more sophisticated arrangement would be needed in a prototype installation.

The hanging cord has the virtue of great simplicity. As explained in Section 4.1, a developed version of the cord with attached fins (see Figure 6) was also tested and proved very effective. The cords do not prevent the early formation of a vortex, and in fact will not be drawn towards the core until it reaches a certain strength. The effectiveness of the cord with fins was such that the vortex did not usually last long enough for the necessary measurements to be taken, and for this reason it does not appear in the above ranking. However, the results in Table 4 shows that this design reduced the proportionate time that vortex motion occurred to about 1% compared with an average of about 45% for the plain projecting pipe. It is therefore likely that the hanging cord with fins belongs well up in the list of effective inhibitors. To gain experience of its performance at full scale, it is suggested that a weighted steel-link chain with attached fins could initially be installed as a remedial measure in a pumping station subject to vortex problems.

The designs of inhibitor which influenced the flow only locally at the intake face (eg the cruciforms and the small fins) were not very effective. Increasing the flow resistance along the floor of the tank by adding the roughness board did not prevent the formation of a surface vortex. Changing the cross-sectional shape of a horizontal intake from circular to square has a small but worthwhile effect ; the position of a vortex core entering a square intake may be less stable than it is in a circular one.

5.2 Intake losses

Vortices produce non-uniform flow conditions in intakes and can therefore give rise to additional head losses. As described in Section 4.3, the measurements of static pressure in the intake were analysed to determine the energy gradient i along the pipe and the head loss coefficient k_i at the entrance (see Tables 5a, b, c, d). The effect of vortex strength and intake geometry on the inlet conditions can therefore be demonstrated by comparing values of i and k_i for the four configurations which were tested : plain pipe, vertical headwall, hooded screen, and vertical headwall plus hooded screen.

It was explained in 4.3 that the tappings in the side of the intake gave significantly different energy gradients from those in the invert. Therefore, the values of i and k_i obtained from the side and bottom tappings have been meaned for the purpose of the following comparisons.

Figures 10 a, b, c, and d show, for each inlet configuration, how the mean energy loss coefficient k_i varies with Reynolds number (R_e=VD/ν). It can be seen that most of the data follow a well-defined trend, and that variations in the water depth have little effect. The values of k_i obtained at the lowest flow rates (< 4l/s in the small tank) show the most scatter, probably because the corresponding energy gradients were too small to be measured very accurately. For values of R_e $>10^5$, the head loss coefficient tends to decrease gradually with increasing discharge, even though the vortex motion is then becoming stronger (see Table 5). The experimental arrangement did not allow the necessary pressure measurements to be made at flow rates sufficient to produce air-entraining vortices. However, the results show that vortices up to strength 3 and 4 do not produce any measurable increase in head loss at the entrance to an intake. A similar conclusion also applies to the energy gradient in the downstream pipe.

The effect of intake configuration on head losses can be seen by comparing differences in the overall values of the entry loss coefficent k_i for each design. Table 9 gives the overall mean value of k_i and the associated standard deviation for each intake, calculated using the data for both side and bottom tappings but omitting tests carried out at flow rates below 4 l/s (since these were considered less reliable). Equivalent results are also given for the ratio between the mean energy gradient i in the pipe and the gradient i_{cw} calculated from the Colebrook-White resistance formula (using an assumed roughness of k_s=0.003mm).

In the case of the entry loss coefficients k_i, it can be seen from Table 9 that the values are all close to the expected orifice coefficient of about 0.6. Adding the headwall to the plain pipe improved the approach conditions by eliminating re-entrant flows ; the benefit is seen in terms of a small reduction in k_i from 0.584 to 0.548. Adding the hooded screen to the plain pipe also helped to straighten the approaching flow, and this may have reduced the entrance loss slightly ; set against this, however, was the additional head loss experienced by the flow passing through the bar screens (mounted above and around the sides of the intake but not across its face). Overall, the mean entrance loss for the hooded screen was found to be almost identical with that for the plain pipe. Adding the hooded screen to the headwall is unlikely to have improved the approach conditions much further, but the bars would have produced some extra head losses; this may explain why the mean value of k_i increased slightly from 0.586 to 0.619. Overall, the differences in the performance of the four configurations are small and of the same order as the standard deviations in the individual values of k_i.

In the case of the energy gradient i in the pipe downstream of the entrance, it is remarkable how close the mean values are to the gradients predicted by the Colebrook-White equation (see Table 9). As explained in Section 4.2, the comparison is based on the mean of the gradients determined from the separate tappings in the side and bottom of the pipe ; Table 5 shows that the bottom tappings gave considerably larger gradients than the side tappings. This difference is believed to have been due to the non-uniform velocity distribution in the pipe caused by the contraction of the flow at the entrance and by the swirl associated with any vortex action. The close agreement between the measurements and the predicted values may be slightly fortuitous, but suggests that the Colebrook-White equation will give reasonable estimates for design. The geometry of the intake does not appear to have any significant effect on the energy gradient in the downstream pipe. The results also indicate that care is needed when measuring head losses in models of intakes ; a single line of tappings along a tunnel could give misleading estimates of the energy gradient.

5.3 Effect of intake geometry

Figures 11a, b, c show how the circulation strength of the vortices in the small tank varied with discharge for two different intake designs : the plain projecting pipe and the extended longitudinal fin of height 2D. Best-fit lines have been drawn through the data for each inhibitor and water level, and these suggest that the circulation strengths with the fin were less than occurred under similar conditions with the plain pipe. However, due to the scatter in the data, this is to some extent a subjective judgement. Therefore, the statistical method of hypothesis testing was used to help decide whether or not the results obtained with the two intake designs were distinct. Considering for example the data in Figure 11a, it can be seen that as the two best-fit lines diverge, it becomes more certain that the two sets of results belong to separate parent populations. A method of applying the Student's t-test was devised which took account of the difference in slope between the two best-fit lines and the standard deviations of the data from these lines. Adopting a 95% confidence limit, it was possible to show that above a certain value of discharge the data for the plain pipe were distinct from the data for the extended fin. The limiting discharges were found to be 0.001 m^3/s at a water level of 0.382m, 0.002 m^3/s at a water level of 0.573m and 0.006 m^3/s at a water level of 0.795m;

these compare with the maximum flow rate of 0.023 m^3/s used in the tests. There is, therefore, good statistical evidence that the data sets for the two intakes are distinct.

Comparing the plots in Figure 11, it can be seen that the ratio of the quantity Γ/Q for a given inhibitor did not vary greatly with water depth ; the overall mean values were:

plain pipe : $\Gamma/Q = 1.25\ m^{-1}$

extended 2D fin: $\Gamma/Q = 0.82\ m^{-1}$

These figures indicate that there is a significant difference in flow behaviour at the two intakes, and that circulation strengths are lower with the more effective inhibitor.

The general conclusion, therefore, is that different inhibitors can experience different strengths of vortex even when the approach conditions and flow rates are the same. This supports the hypothesis described in Section 2.3 that the vortex motion is not determined solely by the approach conditions in the reservoir (as is sometimes supposed), but is also affected by the design of the intake and the local flow conditions which it imposes. If the approaching flow is strongly asymmetric (as perhaps, for example, in a pumping station), the influence of the local intake geometry may be relatively small. However, if an intake is located fairly centrally in a reservoir, the geometry of the intake may be the dominant factor. Therefore, in most cases, vortex problems cannot be solved by considering the overall flow in a reservoir separately from the local flow at the intake. Numerical models can give a general picture of the circulation patterns in a reservoir, but cannot yet describe in sufficient detail how the flow enters an intake ; predictions of circulation strength at the intake may therefore be unreliable. Similarly, results from model tests of an inhibitor may be misleading if they do not take proper account of flow conditions in the reservoir.

A general description of the factors governing the formation of an air-entraining vortex is given in Appendix A. Briefly, it is assumed that this will occur if the flow rate, circulation strength and submergence depth reach certain critical values. The design of the intake influences the circulation strength that develops, but in most cases it does not alter the hydronamic conditions needed to cause an air core to enter the intake. This suggests that data for a wide range of inhibitors will demonstrate a similar relationship between the relevant flow variables. Exceptions may be bar screens which directly disrupt the vortex core, and designs such as hood inlets which significantly increase the length of the core and thereby make it harder for air to reach the intake. The analysis in Appendix A indicates that a modified Kolf number K_1 (taking account of viscous effects, see Equation (A.12)) should depend on the discharge coefficient C and the critical submergence ratio S_c/D. Figures 12a, b and c show all the data from Tables 1 and 2 plotted in the form of K_1 versus C. The results for dimple formation in Figure 12a exhibit a considerable amount of scatter, and this is probably due to the difficulty of measuring very weak vortices that occur only transiently. The data for the material draw-down stage in Figure 12b and the air-core stage in Figure 12c show a more well-defined trend, and give reasonable support to the view that the critical conditions for a given vortex strength are determined principally by the hydrodynamics of the flow.

This contention needs to be tested more rigorously using data from other studies, but let it be assumed that a relationship between the critical flow conditions for an air-core vortex exists as shown diagrammatically in Figure 13. If the values of K_1 and C lie below the critical curve, a continuous air core to the intake will not occur and vice versa. Consider, now the cases described above of the plain pipe and the pipe with the extended longitudinal fin. For the particular reservoir configuration tested, it was found that the circulation strength Γ for the plain pipe increased as the discharge Q increased, but with the ratio Γ/Q remaining approximately constant. This relationship plots in Figure 13 as an almost horizontal line ; where it crosses the critical vortex curve defines the conditions at which an air-core will extend into the intake. Now consider the more "efficient" intake with the longitudinal fin ; this has a lower value of the ratio Γ/Q which crosses the critical vortex curve in Figure 13 at a higher value of C (and hence Q) than the plain pipe.

This example illustrates the general principle suggested by the present study. For a certain class of intake (eg vertical or horizontal), a single hydrodynamic relationship exists between the flow conditions which govern the occurrence of a certain strength of vortex (eg draw of material or formation of air core). However, each combination of reservoir and intake design has its own formula connecting vortex strength, water level and discharge, and this determines in conjunction with the hydrodynamic relationship at what flow rate or water level the specified strength of vortex will occur.

Although this general description may help to explain what happens at an intake, it should be remembered that weak vortices tend to form and die away in an apparently random manner. A diagram such as Figure 13 cannot take these transient effects into account, and can give only an estimate of what is likely to occur.

6 CONCLUSIONS

1. Tests have been carried out in two experimental tanks to compare the effectiveness of thirty different types of vortex inhibitor suitable for horizontal intakes in reservoirs.

2. The inhibitors were compared in terms of the flow rates at which three different strengths of vortex occurred (corresponding to formation of surface dimple, draw of material to the intake, and formation of a continuous air core, see Figure 1).

3. The most efficient type of intake tested was a flush vertical headwall extending above the maximum water level. Adding this headwall to a plain projecting pipe increased the flow rate needed to produce a given strength of vortex by an average ratio of 2.6.

4. Headwalls sloping backwards at 80° to the horizontal and vertical headwalls with slightly projecting pipes were somewhat less effective (average discharge ratios of 2.5 to 2.0). The performance of the headwalls was reduced ocnsiderably if they did not extend to the water surface.

5. Two smaller inhibitors with reasonable performance (discharge ratios about 2.0) were a hooded bar screen and an extended longitudinal fin of height 2D (see Figures 5 and 6). The bars obstructed vortices trying to enter the pipe from

the top and sides. The longitudinal fin straightened the flow and reduced a spiral motion which tended to develop over the intake pipe.

6. Two reasonably efficient low-cost designs that can be easily installed at existing intakes are a floating raft and a newly-developed hanging cord or chain weighted at its end (see Figures 5 and 6). Adding fins to the hanging cord increased its effectiveness considerably, and it is recommended that this device be tested at full size, initially perhaps in a pumping station subject to vortex problems.

7. A square intake is less prone to vortex action than a circular intake having the same cross-sectional area.

8. Installing small fins or cruciforms to straighten the flow entering the intake and roughening the floor of the tank were not very effective at preventing vortex action.

9. Pressures in the intake pipe were measured to determine the effect of vortex strength on head losses for four types of intake (plain pipe, flush headwall, hooded screen and headwall plus hooded screen). Vortex formation was not found to have any adverse effect on entrance loss and friction loss in the pipe for vortices up to strength 4 (the maximum tested here). Varying the geometry of the intake did not change the entrance loss coefficient by more than about ±5% ; the lowest value occurred with the flush headwall. The frictional head loss along the pipe was well predicted by the Colebrook-White equation.

10. The variation of vortex strength with discharge was studied in detail for an "inefficient" intake (plain pipe) and an "efficient" one (pipe with extended fin). For a given discharge, it was that the fin intake experienced a significantly lower vortex strength than the plain pipe. This result shows that the vortex strength which develops at an intake is influenced by the local geometry of the intake and not solely by the approach conditions in the reservoir, as is sometimes supposed. A general description of vortex action at an intake is given in Section 5.3 and Appendix A.

7 ACKNOWLEDGEMENTS

The large experimental tank used in the study was designed and calibrated by Mr A D Crabbe. The majority of the experimental work was carried out by Mr I R Willoughby who also assisted with the analysis. The project was supervised by Mr J A Perkins and Mr R W P May, and was carried out in the River Engineering Department headed by Dr W R White.

8 REFERENCES

ANWAR H.O. (1966). Formation of a weak vortex. Jnl Hydr Res, Vol 4, No.1, pp 1-16.

ANWAR H.O. (1968). Prevention of vortices at intakes. Water Power and Dam Construction, Vol 20, No 10, pp 393-401.

HECKER G.E. (1981). Model-prototype comparison of free surface vortices. Jnl of Hydr Div, Amer Soc Civ Engrs, Vol 107, No 10, pp 1243-1259.

KNAUSS J. (1987). Swirling flow at intakes. Hydraulic Structures Design Manual 1. Intern Assocn Hydr Res, A.A. Balkema, Rotterdam.

PERKINS J.A.P. (1987). Vortex inhibitors. Hydraulics Research, Wallingford, Report SR122.

PROSSER M.J. (1977). The hydraulic design of pump sumps and intakes. BHRA/CIRIA Report No ISBN 0-86017-027-6.

SANMUGANATHAN K. (1986). Air entry in vertical gravity intakes. 5th Congress, Asian and Pacific Regional Division, Intern Assocn Hydr Res, Seoul, Korea, pp 245-264.

STOKES G.G. (1845). On the theories of the internal friction of fluids in motion. Trans Camb Phil Soc, Vol 8, p 287.

TABLES

Table 1 : Performance of inhibitors in Large Tank

Values of (a) Threshold Discharge (m^3/s) (b) Circulation (m^2/s)

Vortex type	Water depth: m		Plain pipe projecting	Headwall 0.61m	Headwall 1.22m	Headwall 1.83m	Headwall 2.44m	Roughness Board	Flush Fin; height 2D	Extended fin; height 2D	Flush Fin; height D	Extended fin; height D	Flush Cruciform;	Extended Cruciform;	Diagonal Extended cruciform	Square Intake
Dimple	1.2	(a)	0.022	0.031	-	0.030	0.043	0.025	0.038	0.045	0.039	0.037	0.051	0.030	0.043	0.034
		(b)	No data	0.0110	-	0.0165	0.0161	0.0137	0.0096	0.0034	0.0046	0.0124	0.0109	0.0190	0.0169	0.0097
	1.8	(a)	0.0423	0.080	0.079	0.075	0.100	0.048	> 0.205	0.106	0.052	0.061	0.090	0.101	0.107	0.048
		(b)	0.0062	0.0146	No Data	0.0214	0.0144	0.0071	No data	0.0312	0.0135	0.0083	0.0090	0.0186	0.0283	0.0152
	2.5	(a)	0.086	0.093	0.083	0.089	0.146	0.114	> 0.205	> 0.205	0.109	0.096	0.104	0.091	0.082	0.097
		(b)	0.0278	0.0191	0.0209	0.0069	0.0161	0.0152	No data	No data	0.0118	No data	0.0323	0.0171	0.0151	0.0075
Material drawn down	1.2	(a)	0.0425	0.057	-	0.063	0.168	0.043	0.092	0.125	0.065	0.076	0.058	0.061	0.059	0.061
		(b)	0.0229	0.0324	-	0.0226	0.0814	0.0310	0.0295	0.0537	0.0133	0.0441	0.0370	0.0341	0.0408	0.0279
	1.8	(a)	0.1362	0.115	0.154	0.109	0.127	0.098	> 0.205	> 0.205	0.100	0.105	0.111	0.109	0.115	> 0.205
		(b)	0.0180	0.0389	0.0573	0.0417	0.0428	0.0332	No data	No data	0.0193	0.0415	0.0424	0.0427	0.0560	No data
	2.5	(a)	0.157	0.165	0.154	> 0.205	> 0.205	> 0.205	> 0.205	> 0.205	0.121	0.145	0.172	0.168	0.136	> 0.205
		(b)	0.0540	0.0524	0.0434	No data	No data	No data	No data	No data	0.0226	0.0579	0.0660	0.0497	0.0778	No data
Air-core	1.2	(a)	0.0856	0.115	> 0.205	0.162	> 0.205	0.067	0.136	> 0.205	0.083	0.085	0.065	0.079	0.077	0.069
		(b)	0.0416	0.0726	No data	0.0641	No data	0.0494	0.0539	No data	0.0286	0.0474	0.0441	0.0480	0.0489	0.0545
	1.8	(a)	0.180	0.176	> 0.205	> 0.205	> 0.205	0.130	> 0.205	> 0.205	> 0.205	0.157	0.155	0.177	0.139	> 0.205
		(b)	0.0328	0.0667	No data	No data	No data	0.0661	No data	No data	No data	0.0775	0.0704	0.0663	0.0621	No data
	2.5	(a)	0.1926	0.183	> 0.205	> 0.205	> 0.205	> 0.205	> 0.205	> 0.205	> 0.205	> 0.205	> 0.205	> 0.205	0.178	> 0.205
		(b)	0.0962	0.0773	No data	No data	No data	No data	No data	No data	No data	No data	No data	No data	0.1271	No data

> 0.205 indicates that the particular vortex type could not be produced for that combination of water depth and intake geometry

Table 2 : Performance of inhibitors in small tank (stage 1 tests)

Values of (a) Threshold Discharge (m^3/s) (b) Circulation (m^2/s)

Vortex type	Water depth: m		Plain pipe projecting	Vertical Headwall Flush	Vertical Headwall (100mm back)	Vertical Headwall (100mm back and Fin Height D)	Vertical Headwall (200mm back)	Vertical Headwall (300mm back)	Headwall at 1 in 3 slope	Sloping (80°) Headwall Flush	Sloping (80°) Headwall (100mm back)	Sloping (80°) Headwall (200mm back)	Flush Fin Height 2D	Flush fin Height D	Extended Fin Height 2D	Series of individual Fins Height 2D	Raft 'D' square	Raft '3/2D' square	Raft '3/2D' square with keel	Cruciform flush	Screen above intake 'D' Square
Dimple	0.382	(a)	0.0023	0.0141	0.0122	0.0128	0.0092	0.0082	0.0075	0.0090	0.0082	0.0075	0.0046	0.0045	0.0069	0.0063	0.0074	0.0080	0.0070	0.0040	0.0059
		(b)	0.0041	0.0054	0.0059	0.0098	0.0036	0.0088	0.0077	0.0040	0.0040	0.0055	0.0037	0.0048	0.0076	0.0071	0.0102	0.0078	0.0074	0.0080	0.0059
	0.573	(a)	0.0067	0.0169	0.0162	0.0167	0.0126	0.0146	0.0082	0.0158	0.0129	0.0108	0.0089	0.0072	0.0113	0.0111	0.0144	0.0106	0.0100	0.0086	0.0085
		(b)	0.0051	0.0065	0.0085	0.0037	0.0025	0.0170	0.0036	0.0043	0.0033	0.0054	0.0109	0.0077	0.0069	0.0108	0.0108	0.0103	0.0043	0.0049	0.0057
	0.795	(a)	0.0077	> 0.0263	> 0.0263	> 0.0263	0.0207	0.0118	0.0117	0.0182	0.0160	0.0185	0.0179	0.0082	0.0123	0.0116	0.0125	0.0112	0.0127	0.0117	0.0116
		(b)	0.0059	No data	No data	No data	0.0058	0.0037	0.0068	0.0072	0.0047	0.0063	0.0078	0.0076	0.0112	0.0115	0.0070	0.0102	0.0112	0.0064	0.0066
Material drawn down	0.382	(a)	0.0121	> 0.0263	0.0245	0.0245	0.0211	0.0146	0.0137	0.0220	0.0209	0.0193	0.0135	0.0125	0.0159	0.0126	0.0135	0.0122	0.0121	0.0143	0.0141
		(b)	0.0159	No data	0.0173	0.0181	0.0205	0.0170	0.0163	0.0097	0.0107	0.0121	0.0145	0.0123	0.0240	0.0176	0.0170	0.0154	0.0151	0.0145	0.0141
	0.573	(a)	0.0127	> 0.0263	> 0.0263	> 0.0263	> 0.0263	> 0.0263	0.0239	> 0.0263	> 0.0263	> 0.0263	0.0178	0.0162	0.0216	> 0.0263	0.0196	0.0200	0.0168	> 0.0263	0.0160
		(b)	0.0221	No data	No data	No data	No data	No data	0.0135	No data	No data	No data	0.0184	0.0233	0.0240	No data	0.0173	0.0212	0.0147	No data	0.0125
	0.795	(a)	0.0146	> 0.0263	> 0.0263	> 0.0263	> 0.0263	> 0.0263	> 0.0263	> 0.0263	> 0.0263	> 0.0263	> 0.0263	0.0205	> 0.0263	0.0234	0.0170	0.0229	0.0203	> 0.0263	0.0211
		(b)	0.0215	No data	No data	No data	No data	No data	No data	No data	No data	No data	No data	0.0261	No data	0.0353	0.0189	0.0261	0.0198	No data	0.0174
Air core	0.382	(a)	0.0154	> 0.0263	> 0.0263	> 0.0263	> 0.0263	0.0199	0.0191	> 0.0263	> 0.0263	0.0233	0.0159	0.0158	0.0199	0.0216	0.0154	0.0143	0.0149	0.0166	0.0172
		(b)	0.0242	No data	No data	No data	No data	0.0246	0.0308	No data	No data	0.0196	0.0197	0.0251	0.0320	0.0300	0.0238	0.0221	0.0228	0.0209	0.0228
	0.573	(a)	0.0170	> 0.0263	> 0.0263	> 0.0263	> 0.0263	> 0.0263	> 0.0263	> 0.0263	> 0.0263	> 0.0263	0.0242	0.0241	> 0.0263	> 0.0263	0.0232	0.0222	0.0229	> 0.0263	0.0243
		(b)	0.0261	No data	No data	No data	No data	No data	No data	No data	No data	No data	0.0261	0.0262	No data	No data	0.0298	0.0207	0.0230	No data	0.0213
	0.795	(a)	0.0232	> 0.0263	> 0.0263	> 0.0263	> 0.0263	> 0.0263	> 0.0263	> 0.0263	> 0.0263	> 0.0263	> 0.0263	0.0243	> 0.0263	> 0.0263	0.0230	> 0.0263	> 0.0263	> 0.0263	> 0.0263
		(b)	0.0357	No data	No data	No data	No data	No data	No data	No data	No data	No data	No data	0.0339	No data	No data	0.0245	No data	No data	No data	No data

> 0.0263 indicates tht the particular vortex type could not be produced for that combination of water depth and intake geometry

TABLE 3 : PERFORMANCE OF INHIBITORS IN SMALL TANK (STAGE 2 TESTS)

VALUES OF (A) THRESHOLD DISCHARGE (m3/s) ; (B) CIRCULATION (m2/s)

VORTEX TYPE	WATER DEPTH m	VERTICAL CORD (NO FINS)	SQUARE INTAKE	HOODED BAR SCREEN
DIMPLE	0.382 (A)	0.0071	0.0036	0.0065
	(B)	0.0045	0.0058	0.0124
	0.573 (A)	0.0090	0.0082	0.0098
	(B)	0.0059	0.0069	0.0061
	0.795 (A)	0.0111	0.0105	0.0118
	(B)	0.0045	0.0055	0.0079
MATERIAL DRAW DOWN	0.382 (A)	0.0157	0.0132	0.0229
	(B)	0.0169	0.0094	0.0335
	0.573 (A)	>0.0263	0.0186	0.0240
	(B)	No data	0.0169	0.0203
	0.795 (A)	0.0190	0.0226	>0.0263
	(B)	0.0193	0.0170	No data
AIR CORE	0.382 (A)	0.0236	0.0159	>0.0263
	(B)	0.0256	0.0139	No data
	0.573 (A)	>0.0263	0.0216	>0.0263
	(B)	No data	0.0180	No data
	0.795 (A)	>0.0263	0.0239	>0.0263
	(B)	No data	0.0257	No data

>0.0263 indicates that the particular vortex type could not be produced for that combination of water depth and intake geometry.

TABLE 4 : PERFORMANCE OF HANGING CORD INHIBITOR (WITH FINS) IN SMALL TANK

WATER DEPTH m	DISCHARGE m3/s	VORTEX STRENGTH	TIME VORTEX PRESENT (per centage)	
			(A) without cord	(B) with cord
0.795	0.02210	4/5	47.75	0.63
	0.02352	5/6	25.60	0.67
0.573	0.01655	4/5	37.03	0.77
	0.02192	5/6	35.67	1.33
	0.02399	6	36.30	0.93
0.382	0.01270	4/5	55.87	4.17
	0.02123	6	66.33	0.22
	0.02446	6+	66.37	0.27

TABLE 5a : HEAD LOSS DATA FOR PLAIN PIPE

DISCHARGE m3/s	ENERGY GRADIENT i C-WHITE	MEASURED i SIDE TAPPINGS	MEASURED i BOTTOM TAPPINGS	MEAN MEASURED i	HEAD LOSS COEFF SIDE TAPPINGS	HEAD LOSS COEFF BOTTOM TAPPINGS	REYNOLDS NUMBER	MEAN AREA COEFF	VORTEX STRENGTH
WATER DEPTH = 0.795 m									
0.0021	0.0081	0.0067	0.0135	0.0101	1.7106	1.6150	36877	0.9774	0
0.0042	0.0278	0.0169	0.0388	0.0278	0.6232	0.5507	73572	0.6916	0
0.0053	0.0426	0.0303	0.0607	0.0455	0.6626	0.5999	93251	0.6812	0
0.0072	0.0753	0.0539	0.1113	0.0826	0.6428	0.5837	127818	0.6871	1
0.0078	0.0866	0.0911	0.1247	0.1079	0.6433	0.6071	138102	0.6876	2
0.0094	0.1213	0.0877	0.1686	0.1281	0.6204	0.5734	166287	0.6924	2
0.0111	0.1654	0.1180	0.2192	0.1686	0.5722	0.5272	197140		2
0.0122	0.1944	0.1382	0.2596	0.1989	0.5828	0.5337	215399		2
0.0124	0.2026	0.1450	0.2866	0.2158	0.5799	0.5270	220362		2
WATER DEPTH = 0.573 m									
0.0026	0.0121	0.0101	0.0152	0.0126	0.5234	0.4964	46095	0.7179	0
0.0042	0.0282	0.0202	0.0388	0.0295	0.5865	0.5360	74102	0.6963	0
0.0060	0.0539	0.0337	0.0809	0.0573	0.6285	0.5656	106194	0.6890	3
0.0068	0.0683	0.0472	0.0995	0.0733	0.6326	0.5755	121082	0.6861	3
0.0080	0.0915	0.0607	0.1349	0.0978	0.6385	0.5759	142358	0.6925	3
0.0086	0.1026	0.0708	0.1517	0.1113	0.6386	0.5733	151576	0.7099	4
0.0086	0.1026	0.0640	0.1450	0.1045	0.6364	0.5772	151576	0.6896	3
0.0089	0.1094	0.0775	0.1517	0.1146	0.6393	0.5895	157075	0.6924	3
0.0089	0.1094	0.0775	0.1551	0.1163	0.6264	0.5715	157075	0.7082	4
0.0089	0.1094	0.0742	0.1618	0.1180	0.6306	0.5670	157075	0.7073	4
0.0111	0.1638	0.1045	0.2192	0.1618	0.5582	0.5067	196074		3
0.0111	0.1643	0.1079	0.2259	0.1669	0.5665	0.5179	196427		3
WATER DEPTH = 0.382 m									
0.0016	0.0049	0.0034	0.0067	0.0051	0.2825	0.2499	27654	0.7984	0
0.0022	0.0090	0.0067	0.0135	0.0101	0.2825	0.2499	39182	0.7450	3
0.0040	0.0263	0.0202	0.0263	0.0233	0.4917	0.4757	71267	0.7069	3
0.0053	0.0434	0.0304	0.0641	0.0472	0.6514	0.5775	94135	0.6952	3
0.0053	0.0434	0.0303	0.0674	0.0489	0.6447	0.5803	94135	0.6971	3
0.0068	0.0679	0.0438	0.0961	0.0700	0.6087	0.5485	120728	0.7002	3
0.0079	0.0897	0.0674	0.1281	0.0978	0.6560	0.6031	140761	0.6909	3
0.0102	0.1418	0.0877	0.1922	0.1399	0.5744	0.5167	181180		3
0.0102	0.1418	0.0877	0.1922	0.1399	0.5684	0.5100	181180		5

TABLE 5b : HEAD LOSS DATA FOR VERTICAL HEADWALL FLUSH WITH INTAKE

DISCHARGE m3/s	ENERGY GRADIENT i C-WHITE	MEASURED i SIDE TAPPINGS	MEASURED i BOTTOM TAPPINGS	MEAN MEASURED i	HEAD LOSS COEFF SIDE TAPPINGS	HEAD LOSS COEFF BOTTOM TAPPINGS	REYNOLDS NUMBER	MEAN AREA COEFF	VORTEX STRENGTH
WATER DEPTH = 0.795 m									
0.0026	0.0117	0.0084	0.0152	0.0118	0.5970	0.5333	45205	0.7333	0
0.0050	0.0393	0.0287	0.0607	0.0447	0.6500	0.5711	89173	0.6974	0
0.0082	0.0942	0.0759	0.1467	0.1113	0.5873	0.5278	144662	0.7098	1
0.0100	0.1351	0.0944	0.1972	0.1458	0.5366	0.4797	176394	0.7200	1
0.0125	0.2053	0.1382	0.3068	0.2225	0.5461	0.4494	221959		2
WATER DEPTH = 0.573 m									
0.0023	0.0099	0.0067	0.0101	0.0084	0.2923	0.2660	41309	0.7763	0
0.0055	0.0467	0.0320	0.0674	0.0497	0.5869	0.5273	98037	0.7016	1
0.0070	0.0714	0.0540	0.1079	0.0809	0.6394	0.5783	124099	0.6987	2
0.0088	0.1081	0.0759	0.1534	0.1147	0.6062	0.5493	156008	0.7167	2
0.0116	0.1775	0.1214	0.2394	0.1804	0.5480	0.4957	204938		2
0.0116	0.1775	0.1180	0.2546	0.1863	0.5443	0.4795	204938		2
WATER DEPTH = 0.382 m									
0.0025	0.0113	0.0067	0.0152	0.0110	0.4379	0.3909	44321	0.7473	0
0.0053	0.0426	0.0303	0.0641	0.0472	0.5500	0.4856	93251	0.7127	2
0.0066	0.0640	0.0455	0.0944	0.0700	0.6112	0.5509	116832	0.7092	2
0.0081	0.0934	0.0691	0.1332	0.1012	0.5976	0.5457	143955	0.7212	2
0.0107	0.1529	0.0978	0.2225	0.1602	0.5345	0.4716	188807		3

TABLE 5c : HEAD LOSS DATA FOR HOODED BAR SCREEN

DISCHARGE m3/s	ENERGY GRADIENT i C-WHITE	MEASURED i SIDE TAPPINGS	MEASURED i BOTTOM TAPPINGS	MEAN MEASURED i	HEAD LOSS COEFF SIDE TAPPINGS	HEAD LOSS COEFF BOTTOM TAPPINGS	REYNOLDS NUMBER	MEAN AREA COEFF	VORTEX STRENGTH
WATER DEPTH = 0.795 m									
0.0027	0.0125	0.0067	0.0169	0.0118	0.5715	0.4650	46979	0.7777	0
0.0057	0.0488	0.0270	0.0776	0.0523	0.6469	0.5405	100518	0.7446	0
0.0081	0.0932	0.0337	0.1484	0.0910	0.6594	0.5342	143778	0.7544	1
0.0092	0.1178	0.0607	0.1821	0.1214	0.6368	0.5383	163634	0.7479	2
0.0103	0.1426	0.0809	0.2158	0.1484	0.5913	0.5054	181716	0.7540	1
0.0103	0.1426	0.0674	0.2192	0.1433	0.6101	0.5094	181716	0.7526	2
0.0123	0.1976	0.0978	0.3068	0.2023	0.6052	0.5047	217350		2
WATER DEPTH = 0.573 m									
0.0025	0.0113	0.0101	0.0169	0.0135	0.6183	0.5623	44321	0.7545	0
0.0051	0.0408	0.0270	0.0641	0.0455	0.5917	0.5029	90947	0.7534	1
0.0076	0.0836	0.0304	0.1315	0.0809	0.7110	0.5863	135444	0.7532	2
0.0092	0.1160	0.0303	0.1804	0.1054	0.6949	0.5566	162214	0.7595	3
0.0112	0.1673	0.0607	0.2529	0.1568	0.6207	0.5053	198378		3
WATER DEPTH = 0.382 m									
0.0023	0.0095	0.0051	0.0152	0.0101	0.5139	0.4304	40243	0.7895	0
0.0052	0.0415	0.0236	0.0674	0.0455	0.6518	0.5422	91831	0.7503	2
0.0074	0.0791	0.0371	0.1214	0.0792	0.6866	0.5682	131366	0.7594	3
0.0084	0.0989	0.0337	0.1551	0.0944	0.6838	0.5561	148564	0.7585	3
0.0107	0.1534	0.0337	0.2225	0.1281	0.5944	0.4665	189160		3

TABLE 5d : HEAD LOSS DATA FOR VERTICAL HEADWALL AND HOODED BAR SCREEN COMBINED

DISCHARGE m3/s	ENERGY GRADIENT i C-WHITE	MEASURED i SIDE TAPPINGS	MEASURED i BOTTOM TAPPINGS	MEAN MEASURED i	HEAD LOSS COEFF SIDE TAPPINGS	HEAD LOSS COEFF BOTTOM TAPPINGS	REYNOLDS NUMBER	MEAN AREA COEFF	VORTEX STRENGTH
WATER DEPTH = 0.795 m									
0.0033	0.0188	0.0101	0.0270	0.0186	0.6909	0.5806	59038	0.7655	0
0.0051	0.0408	0.0202	0.0641	0.0422	0.6002	0.4812	90947	0.7751	0
0.0076	0.0825	0.0421	0.1382	0.0902	0.6709	0.5545	134378	0.7762	1
0.0095	0.1247	0.0472	0.2124	0.1298	0.6845	0.5461	168774	0.7955	1
0.0111	0.1659	0.0405	0.2225	0.1315	0.7893	0.6891	197494		1
0.0121	0.1929	0.0405	0.2529	0.1467	0.7589	0.6578	214509		1
WATER DEPTH = 0.573 m									
0.0028	0.0138	0.0101	0.0539	0.0320	0.6727	0.2405	49637	0.7000	0
0.0057	0.0493	0.0303	0.0809	0.0556	0.6309	0.5296	101049	0.7295	0
0.0073	0.0774	0.0438	0.1298	0.0868	0.6616	0.5555	129769	0.7311	1
0.0088	0.1076	0.0506	0.1821	0.1163	0.6912	0.5899	155654	0.7582	1
0.0097	0.1285	0.0506	0.2158	0.1332	0.6732	0.5719	171609	0.7763	1
0.0113	0.1706	0.0607	0.2765	0.1686	0.6761	0.5836	200506		2
WATER DEPTH = 0.382 m									
0.0026	0.0117	0.0145	0.0202	0.0174	0.5613	0.5394	45205	0.7289	0
0.0051	0.0408	0.0270	0.0641	0.0455	0.5628	0.4763	90947	0.7323	2
0.0072	0.0753	0.0405	0.1281	0.0843	0.6453	0.5370	127818	0.7368	2
0.0085	0.1019	0.0405	0.1686	0.1045	0.6894	0.5865	151045	0.7742	2
0.0104	0.1464	0.0540	0.2259	0.1399	0.6587	0.5683	184374		3

TABLE 6 DISCHARGE AND CIRCULATION DATA FOR PLAIN PIPE AND LONGITUDINAL FIN INHIBITOR

PLAIN PIPE

WATER LEVEL					
0.795 m		0.573 m		0.382 m	
DISCHARGE m3/s	CIRCULATION m2/s	DISCHARGE m3/s	CIRCULATION m2/s	DISCHARGE m3/s	CIRCULATION m2/s
0.01551	0.01967	0.01611	0.01593	0.00635	0.00547
0.01983	0.01894	0.02202	0.03347	0.01273	0.01719
0.01973	0.01919	0.01122	0.00929	0.01663	0.02166
0.00767	0.00593	0.01128	0.01188	0.02124	0.03218
0.01461	0.02152	0.00671	0.00511	0.00232	0.00412
0.02321	0.03573	0.01266	0.02211	0.01213	0.01588
		0.01699	0.02608	0.01536	0.02421

EXTENDED LONGITUDINAL FIN (2D HIGH)

WATER LEVEL					
0.795 m		0.573 m		0.382 m	
DISCHARGE m3/s	CIRCULATION m2/s	DISCHARGE m3/s	CIRCULATION m2/s	DISCHARGE m3/s	CIRCULATION m2/s
0.02176	0.01279	0.02176	0.01749	0.00567	0.00323
0.02262	0.02059	0.02307	0.02631	0.01116	0.00818
0.02334	0.02099	0.02382	0.02210	0.01474	0.01150
0.01611	0.00759	0.01126	0.00685	0.02049	0.01977
0.01914	0.01012	0.02159	0.02396	0.01593	0.01399
0.01227	0.01124			0.01903	0.01529
				0.00692	0.00756
				** 0.01585	0.02399
				** 0.01986	0.03202

** THESE POINTS NOT USED IN ANY CALCULATIONS

TABLE 7 : DISCHARGE RATIOS FOR INHIBITORS IN LARGE TANK

PIPE DIAMETER D = 0.198 m

INHIBITOR TYPE	DISCHARGE RATIO RELATIVE TO PLAIN PIPE									PERCENTAGE OF MAXIMUM POSSIBLE SCOR
	DIMPLE (STRENGTH 2)			MATERIAL DRAW-DOWN (STRENGTH 4)			AIR CORE (STRENGTH 6)			
S/D	5.18	8.21	11.7	5.18	8.21	11.7	5.18	8.21	11.7	
PLAIN PIPE	1.00	1.00	1.00	1.00	1.00	1.00	1.00	1.00	1.00	100.0
HEADWALL,3D HIGH	1.41	1.90	1.03	1.34	0.85	1.05	1.34	0.98	0.95	64.3
HEADWALL,6D HIGH	1.41	1.64	0.96	1.34	1.07	0.91	>2.39	>1.14	>1.06	59.5
HEADWALL,9D HIGH	1.46	1.77	1.03	1.48	0.80	>1.31	1.89	>1.14	>1.06	42.9
HEADWALL,12D HIGH	1.93	2.36	1.69	3.96	0.93	>1.31	>2.39	>1.14	>1.06	11.9
ROUGHNESS BOARD	1.13	1.12	1.32	1.02	0.72	>1.31	0.80	0.73	>1.06	64.3
FIN,2D HIGH	1.71	>4.85	>2.38	2.19	>1.51	>1.31	1.59	>1.14	>1.06	16.7
FIN,D HIGH	1.75	1.22	1.27	1.54	0.73	0.77	0.97	>1.14	>1.06	85.7
EXTENDED FIN,2D HIGH	2.10	2.52	>2.38	2.93	>1.51	>1.31	>2.39	>1.14	>1.06	14.3
EXTENDED FIN,D HIGH	1.69	1.44	1.12	1.80	0.77	0.93	0.99	0.88	>1.06	47.6
CRUCIFORM	2.33	2.12	1.21	1.36	0.81	1.09	0.77	0.86	>1.06	52.4
EXTENDED CRUCIFORM	1.37	2.40	1.06	1.44	0.80	1.07	0.92	0.99	>1.06	52.4
DIAGONAL CRUCIFORM	1.95	2.53	0.94	1.38	0.84	0.86	0.90	0.78	0.93	64.3
SQUARE INTAKE	1.53	1.15	1.13	1.44	>1.51	>1.31	0.80	>1.14	>1.06	42.9

TABLE 8 : DISCHARGE RATIOS FOR INHIBITORS IN SMALL TANK

PIPE DIAMETER D = 0.063 m

INHIBITOR TYPE	DISCHARGE RATIO RELATIVE TO PLAIN PIPE									PERCENTAGE OF MAXIMUM POSSIBLE SCORE
	DIMPLE (STRENGTH 2)			MATERIAL DRAW-DOWN (STRENGTH 4)			AIR CORE (STRENGTH 6)			
S/D	5.18	8.21	11.7	5.18	8.21	11.7	5.18	8.21	11.7	
PLAIN PIPE	1.00	1.00	1.00	1.00	1.00	1.00	1.00	1.00	1.00	100.0
HEADWALL FLUSH	6.09	2.52	>3.43	>2.17	>2.08	>1.80	>1.71	>1.55	>1.13	4.5
HEADWALL,SET BACK 100mm	5.24	2.41	>3.43	2.02	>2.08	>1.80	>1.71	>1.55	>1.13	10.6
HEADWALL,SET BACK 200mm	3.98	1.88	2.69	1.74	>2.08	>1.80	>1.71	>1.55	>1.13	22.7
HEADWALL,SET BACK 300mm	3.54	1.61	1.53	1.21	>2.08	>1.80	1.30	>1.55	>1.13	40.9
HEADWALL SET BACK 100mm PLUS FIN,D HIGH	5.51	2.49	>3.43	2.02	>2.08	>1.80	>1.71	>1.55	>1.13	9.1
EXTENDED FIN,2D HIGH	2.98	1.68	1.60	1.31	1.71	>1.80	1.29	>1.55	>1.13	50.0
FIN,2D HIGH	1.99	1.33	2.34	1.11	1.41	>1.80	1.04	1.43	>1.13	71.2
FIN,D HIGH	1.92	1.07	1.06	1.03	1.28	1.40	1.03	1.42	1.05	92.4
CRUCIFORM	1.70	1.28	1.53	1.18	>2.08	>1.80	1.08	>1.55	>1.13	59.1
HEADWALL AT 1 IN 3 SLOPE	3.25	1.33	1.52	1.13	1.88	>1.80	1.25	>1.55	>1.13	56.1
SERIES OF FINS,2D HIGH	2.71	1.65	1.52	1.04	>2.08	1.60	1.41	>1.55	>1.13	60.6
HAEDWALL AT 80 ,FLUSH	3.88	2.35	2.38	1.81	>2.08	>1.80	>1.71	>1.55	>1.13	18.2
HEADWALL AT 80 ,SET BACK 100mm	3.55	1.92	2.09	1.72	>2.08	>1.80	>1.71	>1.55	>1.13	24.2
HEADWALL AT 80 ,SET BACK 200mm	3.25	1.61	2.42	1.59	>2.08	>1.80	1.52	>1.55	>1.13	34.8
RAFT,SIDE D	3.20	2.15	1.62	1.11	1.55	1.16	1.00	1.36	0.99	69.7
RAFT,SIDE 3D/2	3.45	1.58	1.46	1.00	1.58	1.57	0.93	1.31	>1.13	63.6
RAFT,SIDE 3D/2 WITH KEEL	3.00	1.49	1.66	1.00	1.33	1.39	0.97	1.35	>1.13	78.8
HANGING CORD (NO FINS)	3.09	1.34	1.44	1.30	>2.08	1.30	1.53	>1.55	>1.13	65.2
SQUARE INTAKE	1.57	1.22	1.36	1.09	1.47	1.55	1.03	1.27	1.03	81.8
SUBMERGED SCREEN D SQUARE	2.53	1.27	1.51	1.16	1.26	1.45	1.12	1.43	>1.03	81.8
FULL HOODED SCREEN	2.83	1.46	1.53	1.89	1.89	>1.80	>1.71	>1.55	>1.13	45.5

TABLE 9 EFFECT OF INTAKE CONFIGURATION ON HEAD LOSSES

INTAKE TYPE	ENTRY LOSS COEFFICIENT k_i		ENERGY GRADIENT RATIO $\bar{i}/i_{cw}$	
	MEAN	STAN. DEV.	MEAN	STAN. DEV.
PLAIN PIPE	0.584	0.037	1.051	0.063
VERTICAL HEADWALL	0.548	0.040	1.087	0.044
HOODED SCREEN	0.586	0.036	0.997	0.076
VERTICAL HEADWALL + HOODED SCREEN	0.619	0.057	1.021	0.117

FIGURES

Vortex strength scale		
1	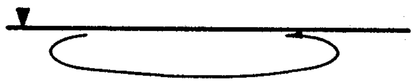	Surface rotation
2		Surface depression with minor dimples. Rotating column of water without significant draw to intake.
3	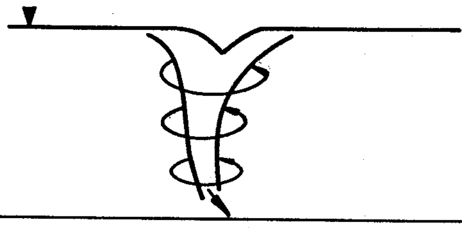	Surface dimple. Rapidly rotating narrow water core with draw to intake.
4	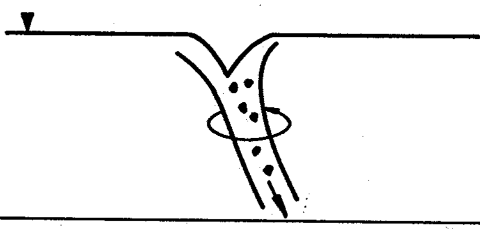	Draw of water and floating trash to intake.
5	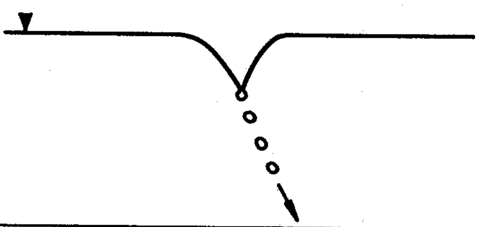	Draw of air bubbles to intake.
6	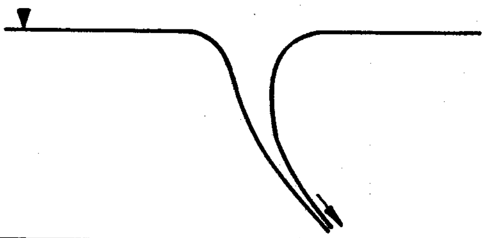	Open air core with continuous air entrainment.

Fig. 1 Vortex strength classification

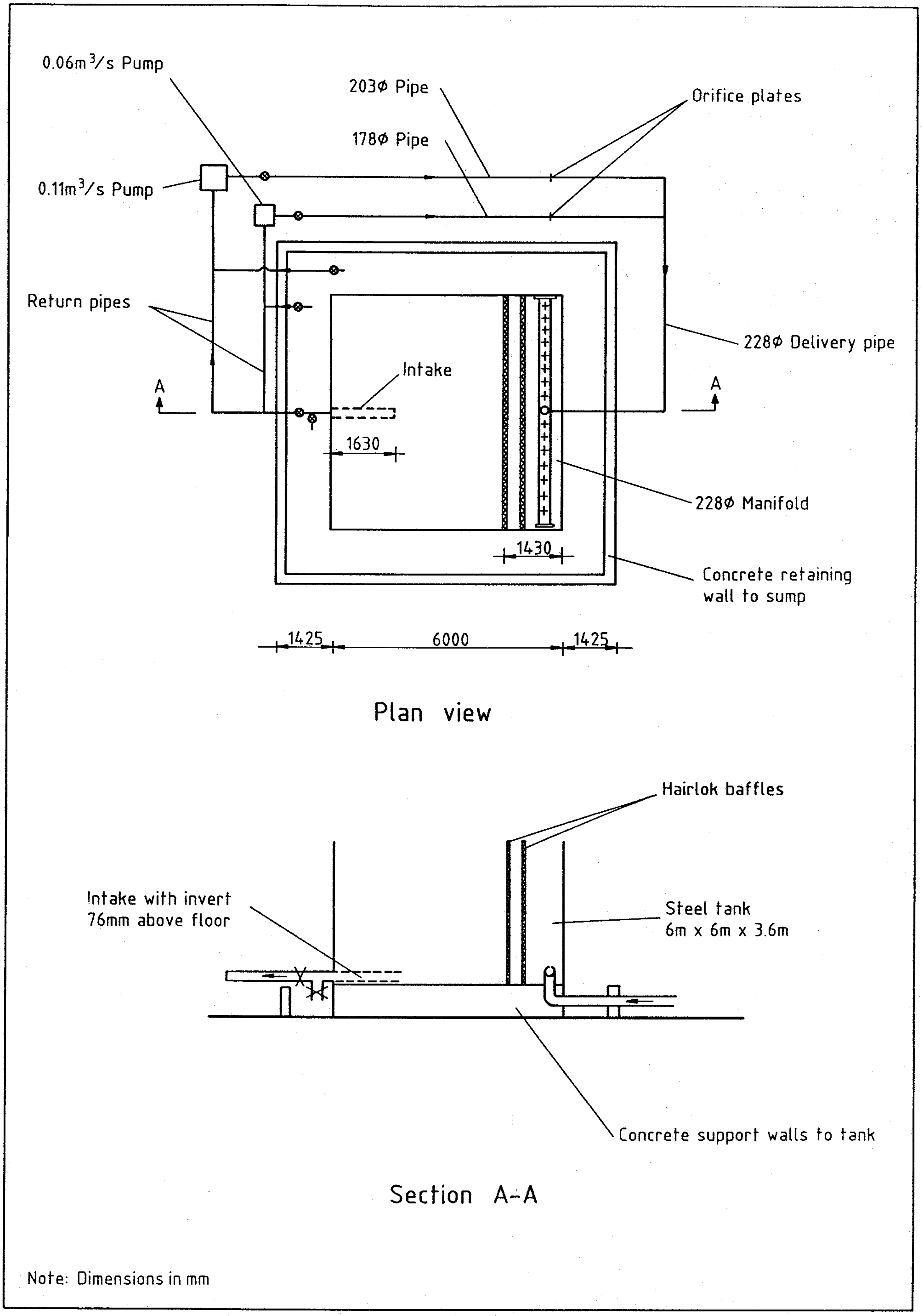

Fig. 2 General layout of large experimental tank

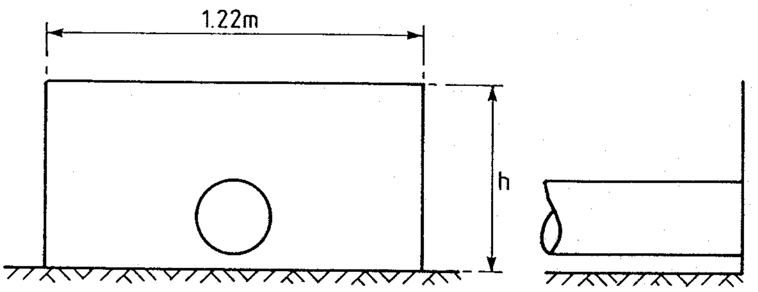

Headwall

Tests carried out with h = 0.61, 1.22, 1.83 and 2.44m respectively

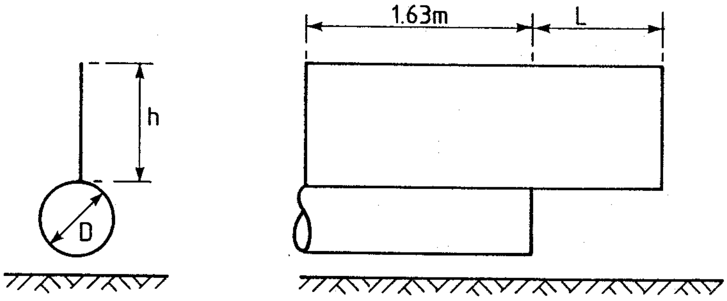

Fin

Tests carried out for

h	L
D	0
D	D
2D	0
2D	2D

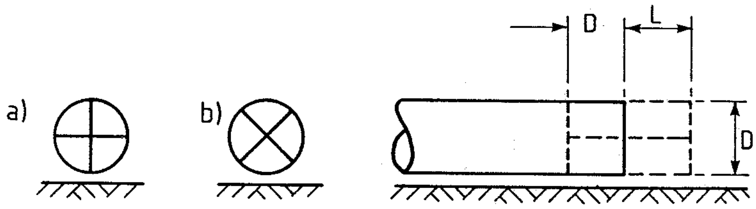

Cruciform

Type a) with L = 0,D
Type b) with L = D

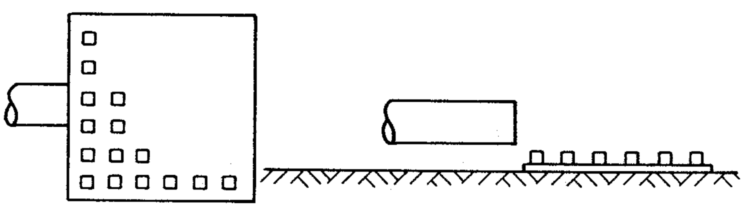

Roughness

Cubes of 50mm side fixed at 200mm centres on base-board 1.22m square

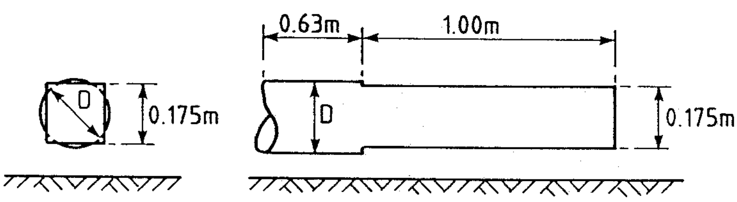

Square section intake

Fig 3 Types of inhibitor : Large tank

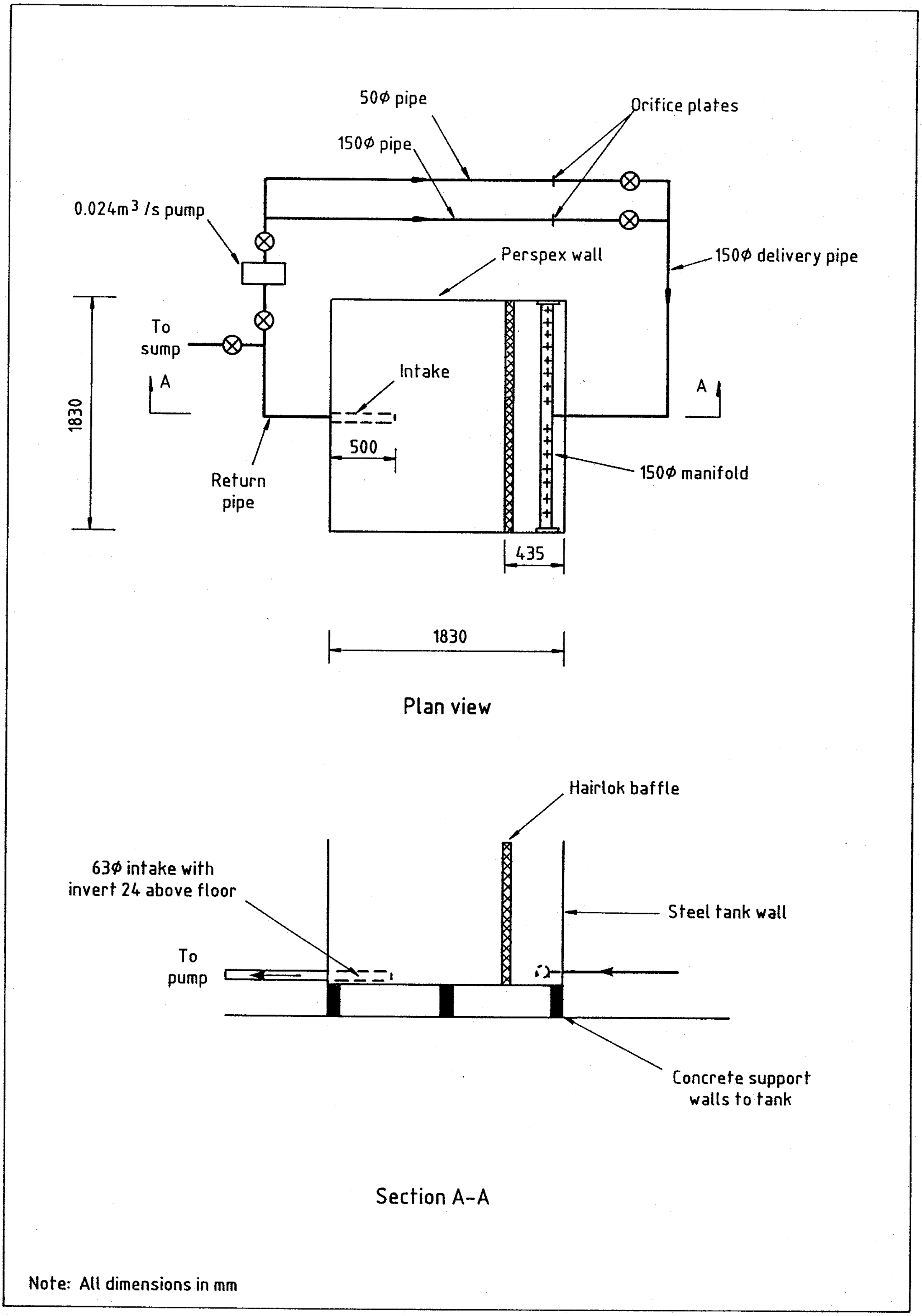

Fig 4 General layout of small experimental tank

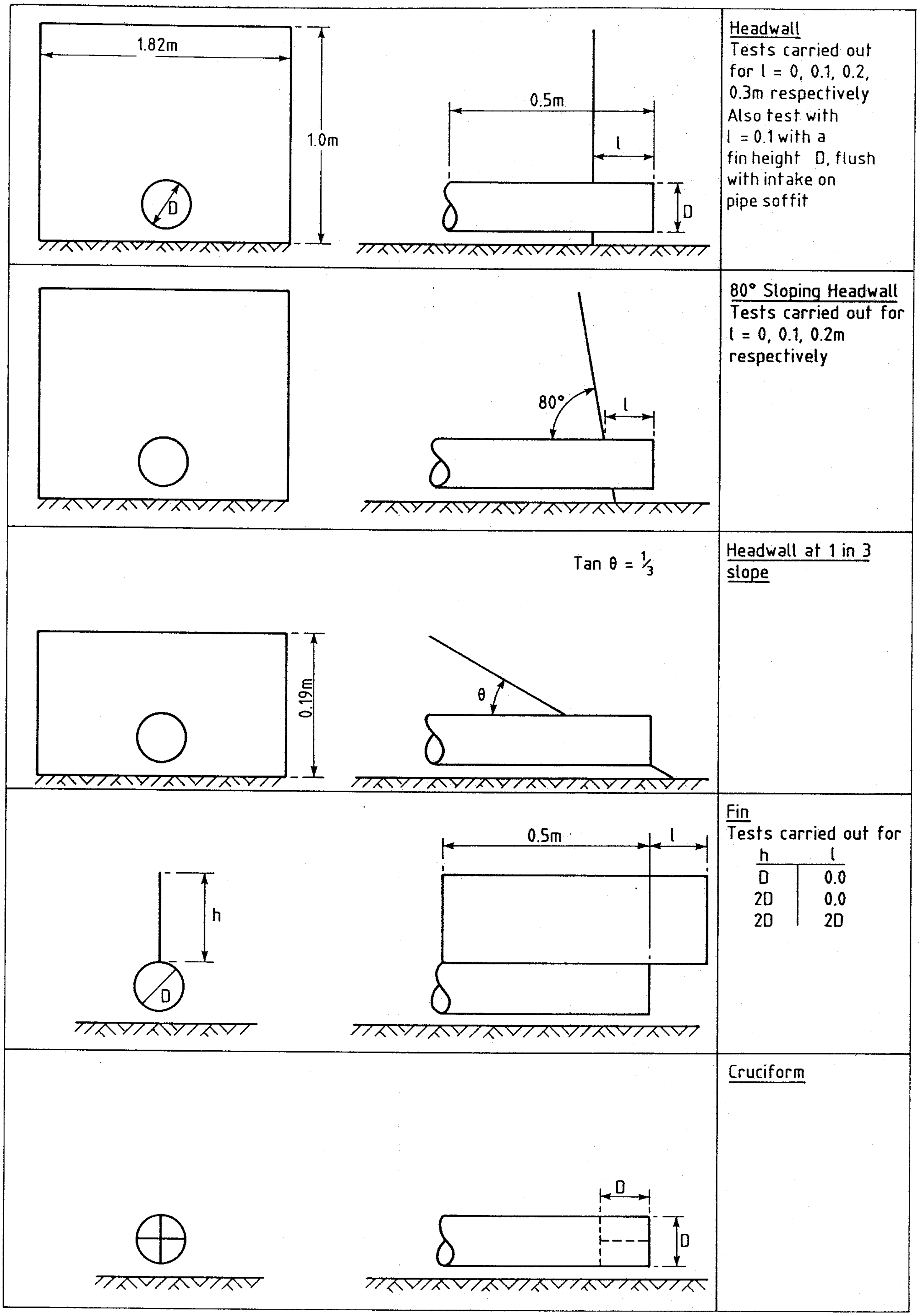

Fig 5 Types of inhibitor : Small tank (Stage 1 tests)

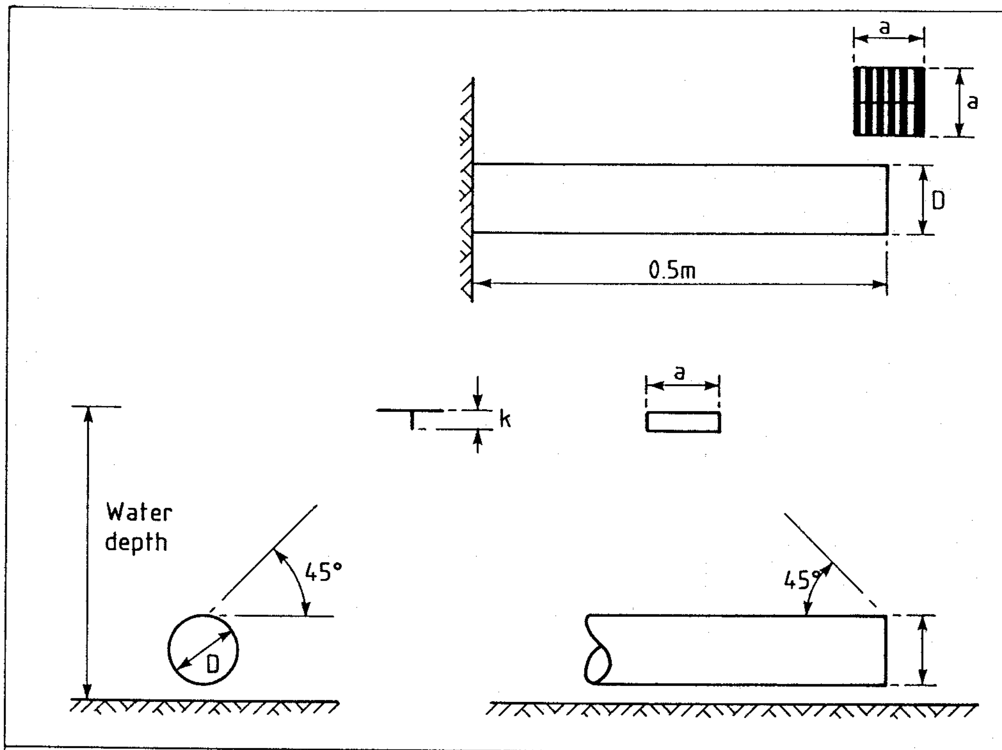

Raft floating on surface

Raft allowed to move freely up to 45° in any direction

Tests carried out with :

k	a
0.0	D
0.0	3D/2
D/2	3D/2

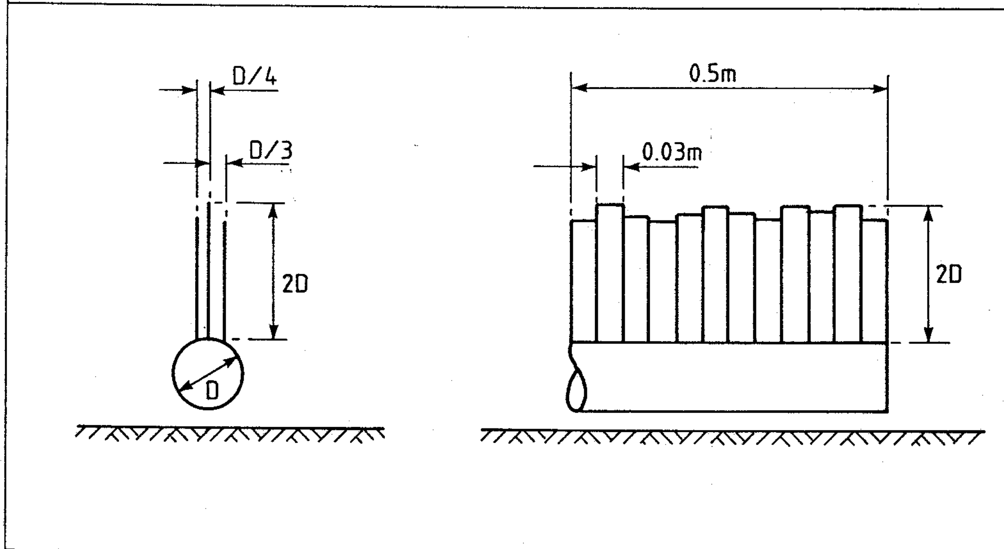

Series of individual fins

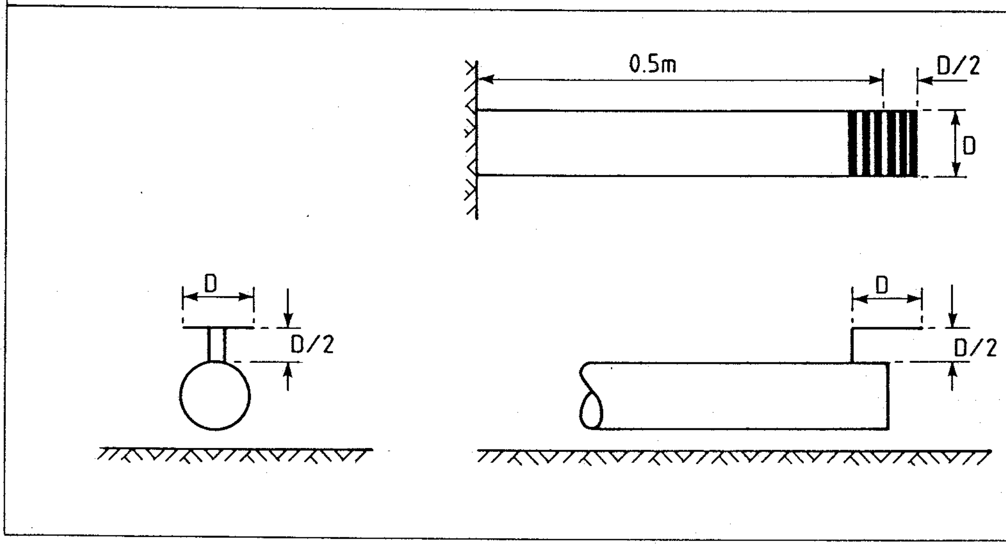

Screen above intake

Fig 5 Types of inhibitor : Small tank (Stage 1 tests)

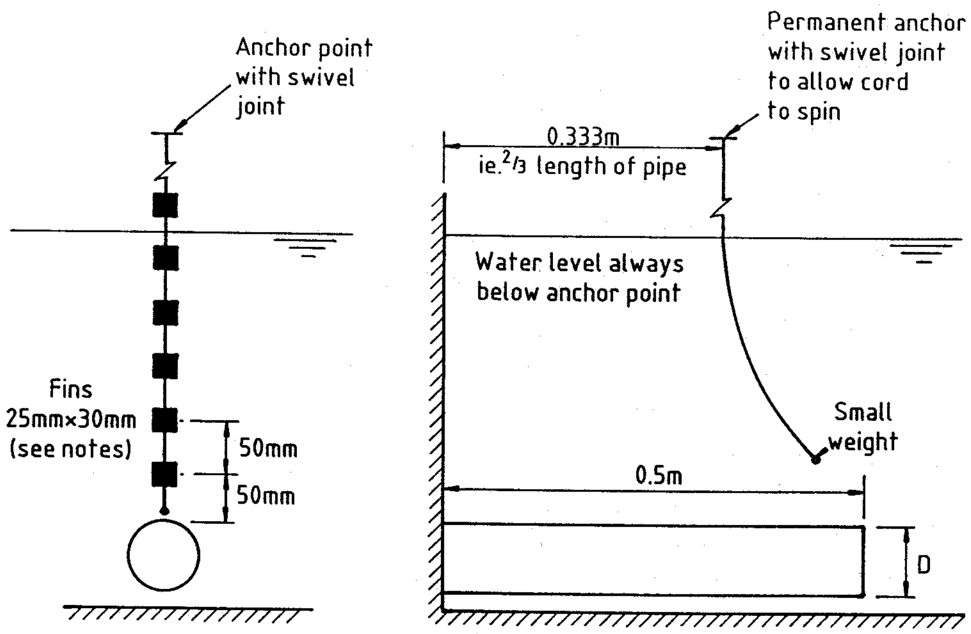

Vertical hanging cord

1.75mm diameter

1.75g/m (mass/unit length)

a) Without fins

small weight = 1.8g

b) With fins

small weight = 1.8g

Weight of fins = approx. 0.3g per fin

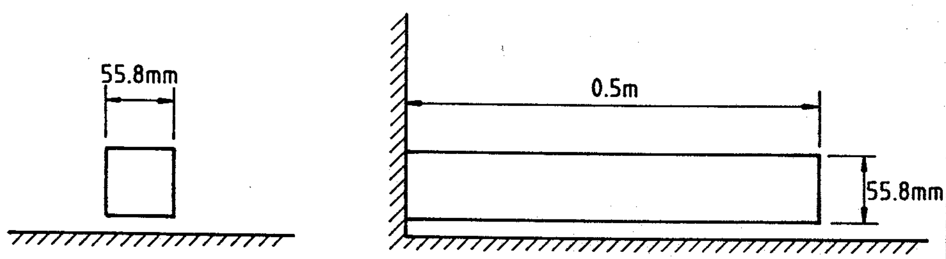

Square section intake

Square intake has same cross-sectional area as circular pipe

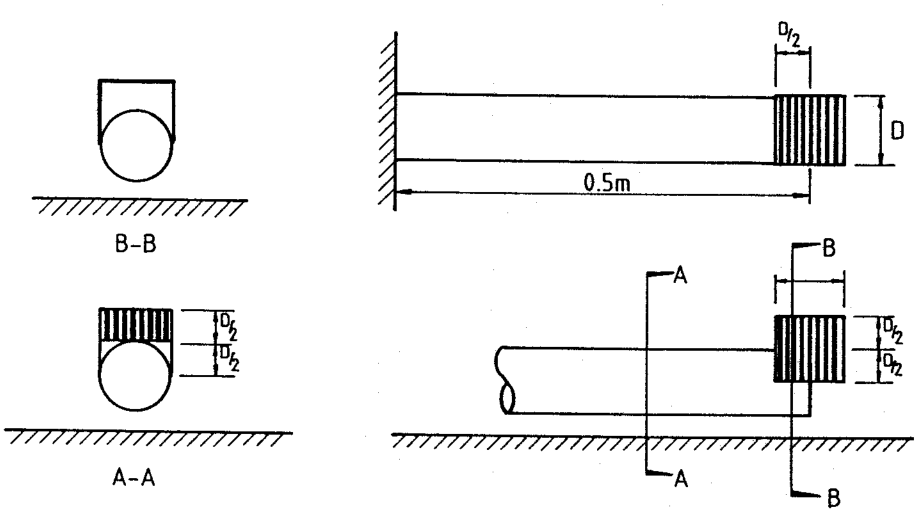

Hooded bar screen

Bars 5mm×3mm ×D or D/2

% opening of screen = 50%

Fig 6 Types of inhibitor : small tank (Stage 2 tests)

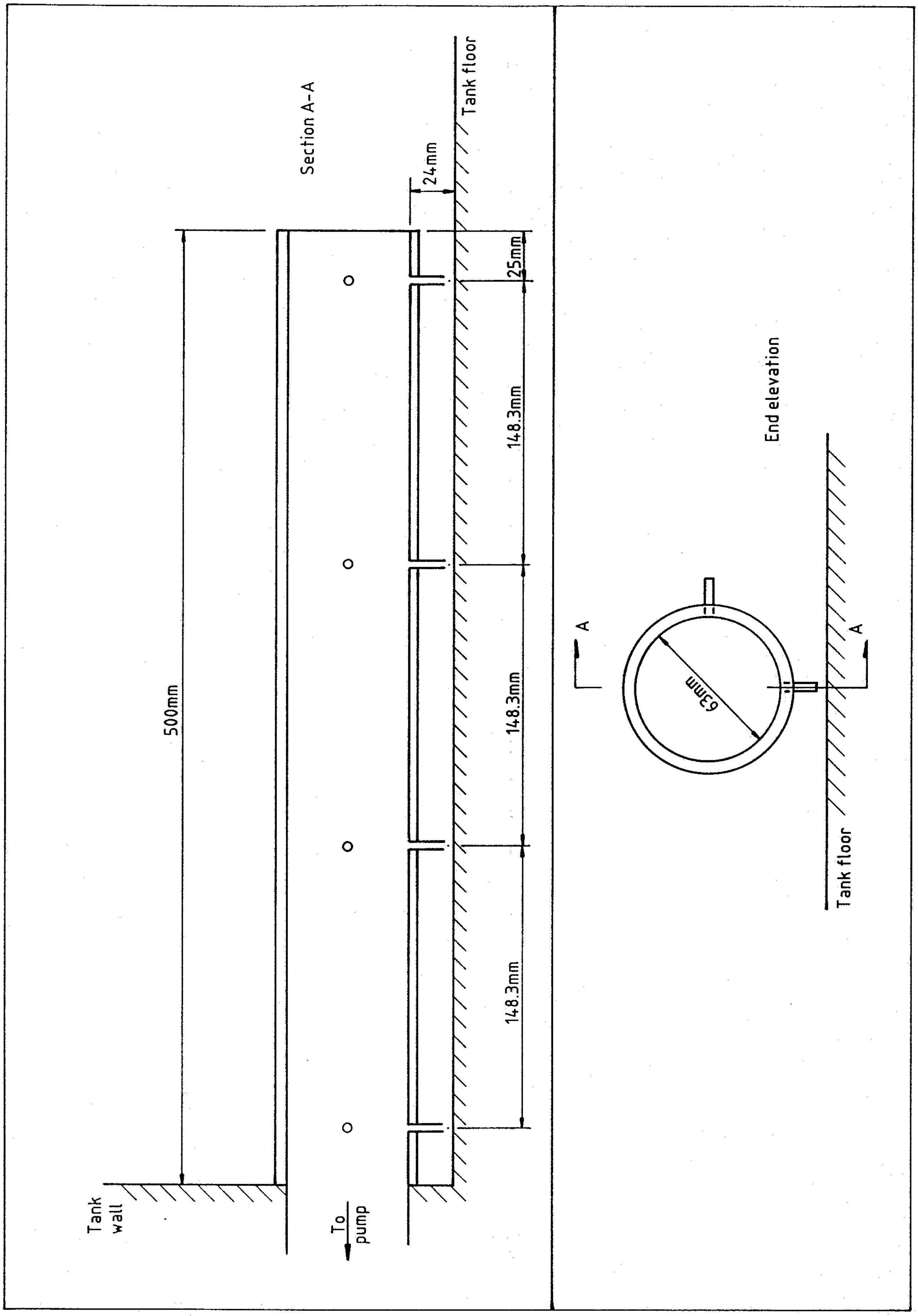

Fig 7 Positions of pressure tappings in intake pipe

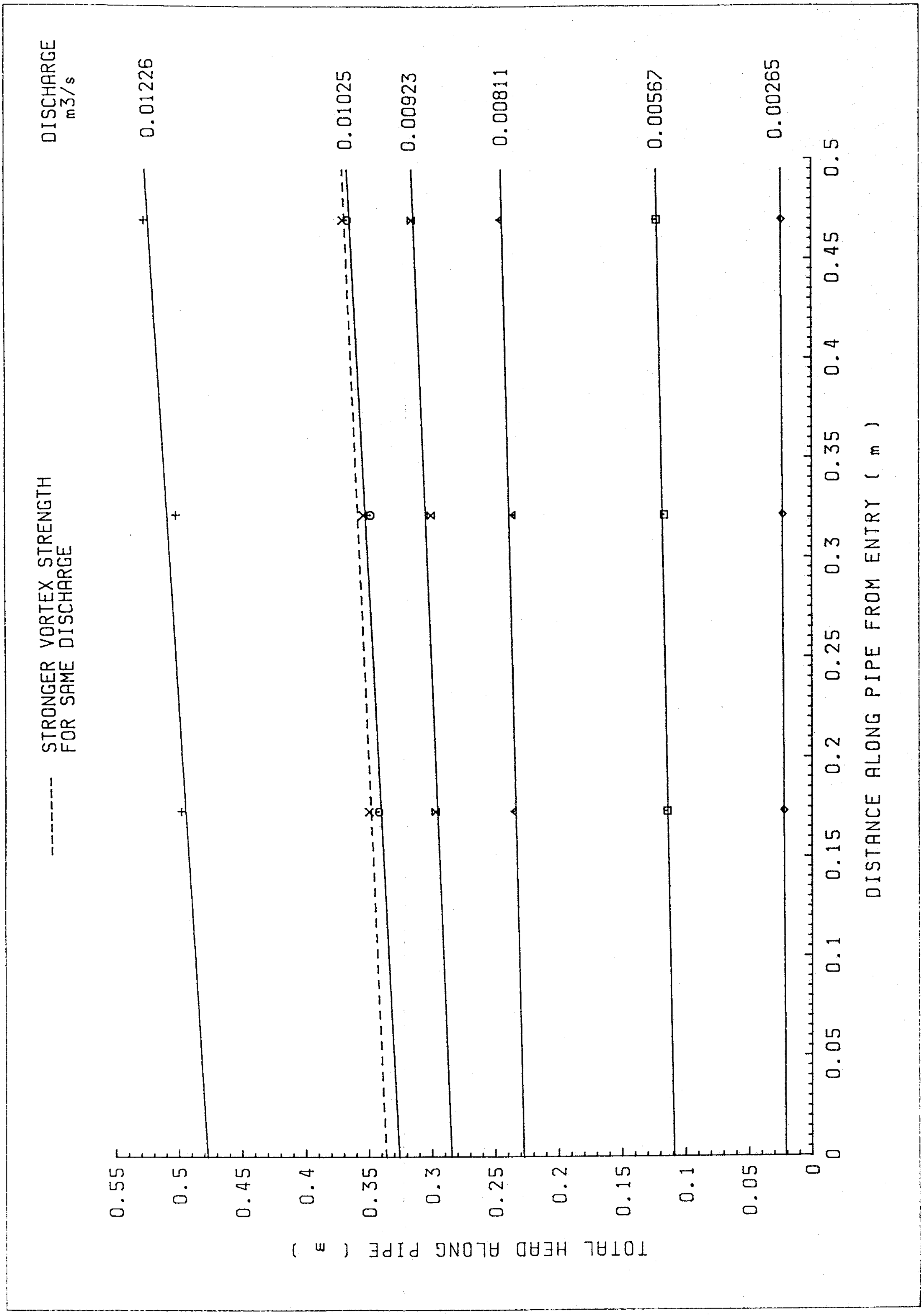

FIG 8 TOTAL HEAD ALONG PIPE WITH HOODED BAR SCREEN
SIDE TAPPINGS WATER DEPTH = 0.795 m

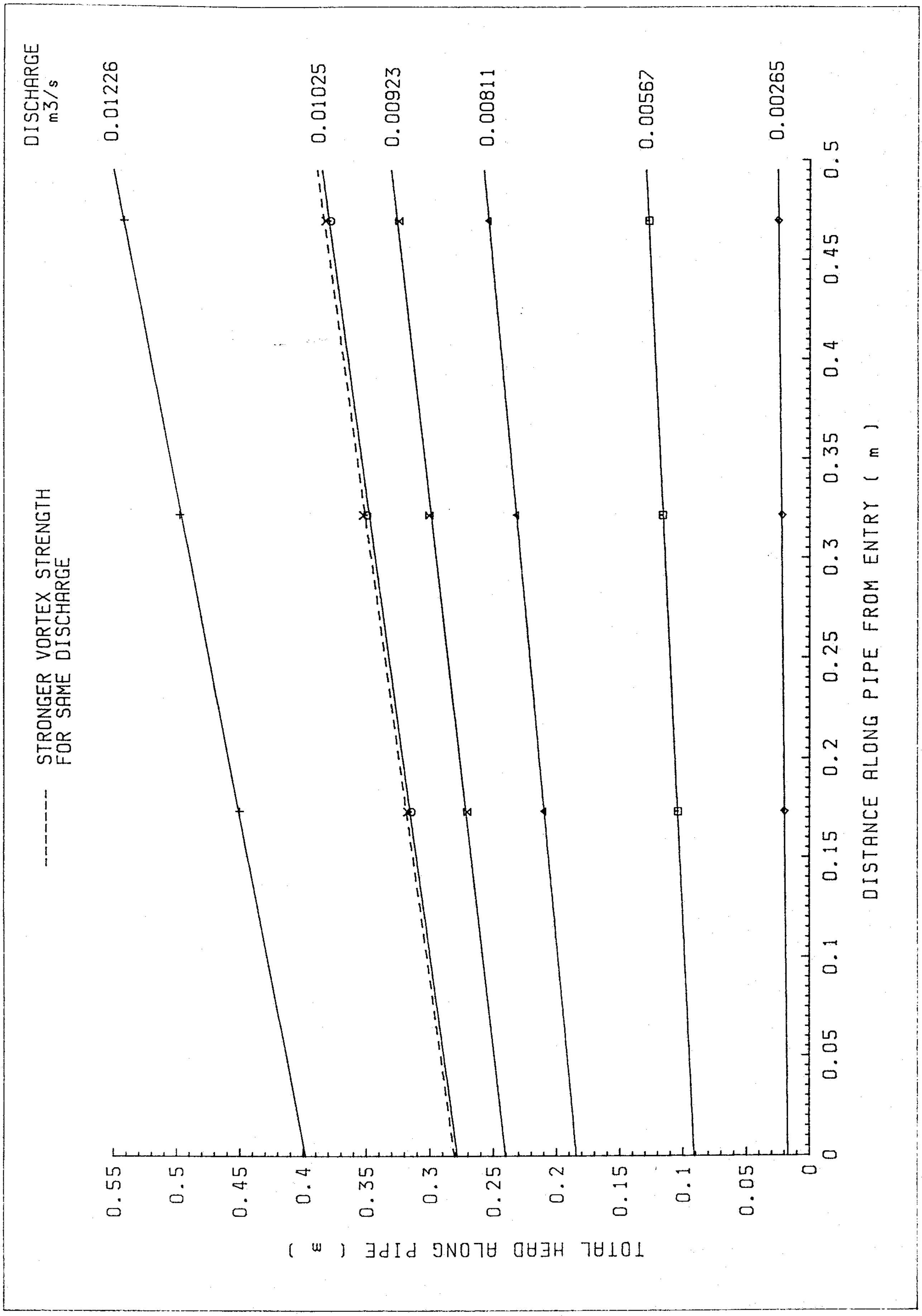

FIG 9 TOTAL HEAD ALONG PIPE WITH HOODED BAR SCREEN
BOTTOM TAPPINGS WATER DEPTH = 0.795 m

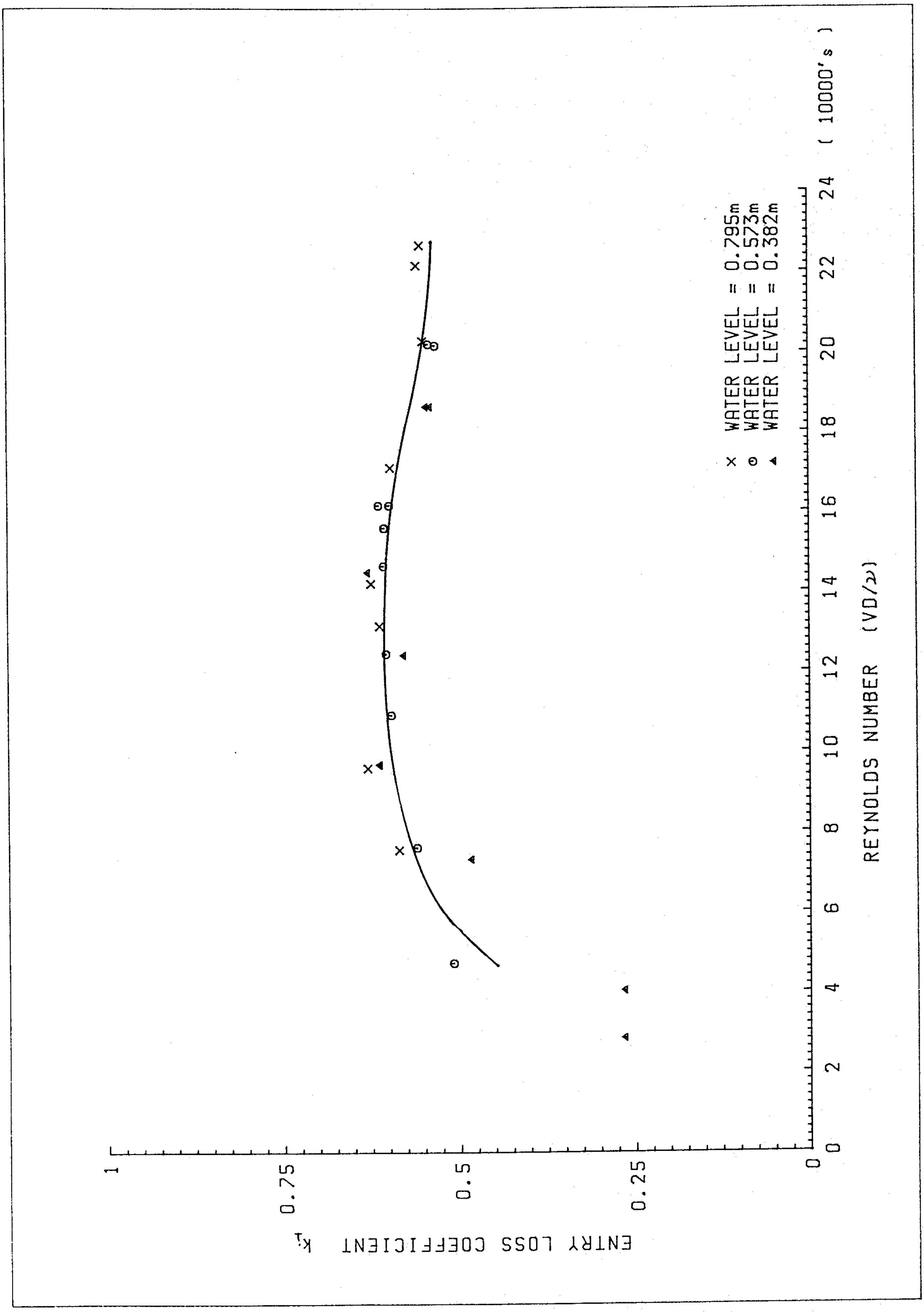

FIG 10a VARIATION OF ENTRY LOSS COEFFICIENT WITH REYNOLDS NUMBER FOR PLAIN PIPE

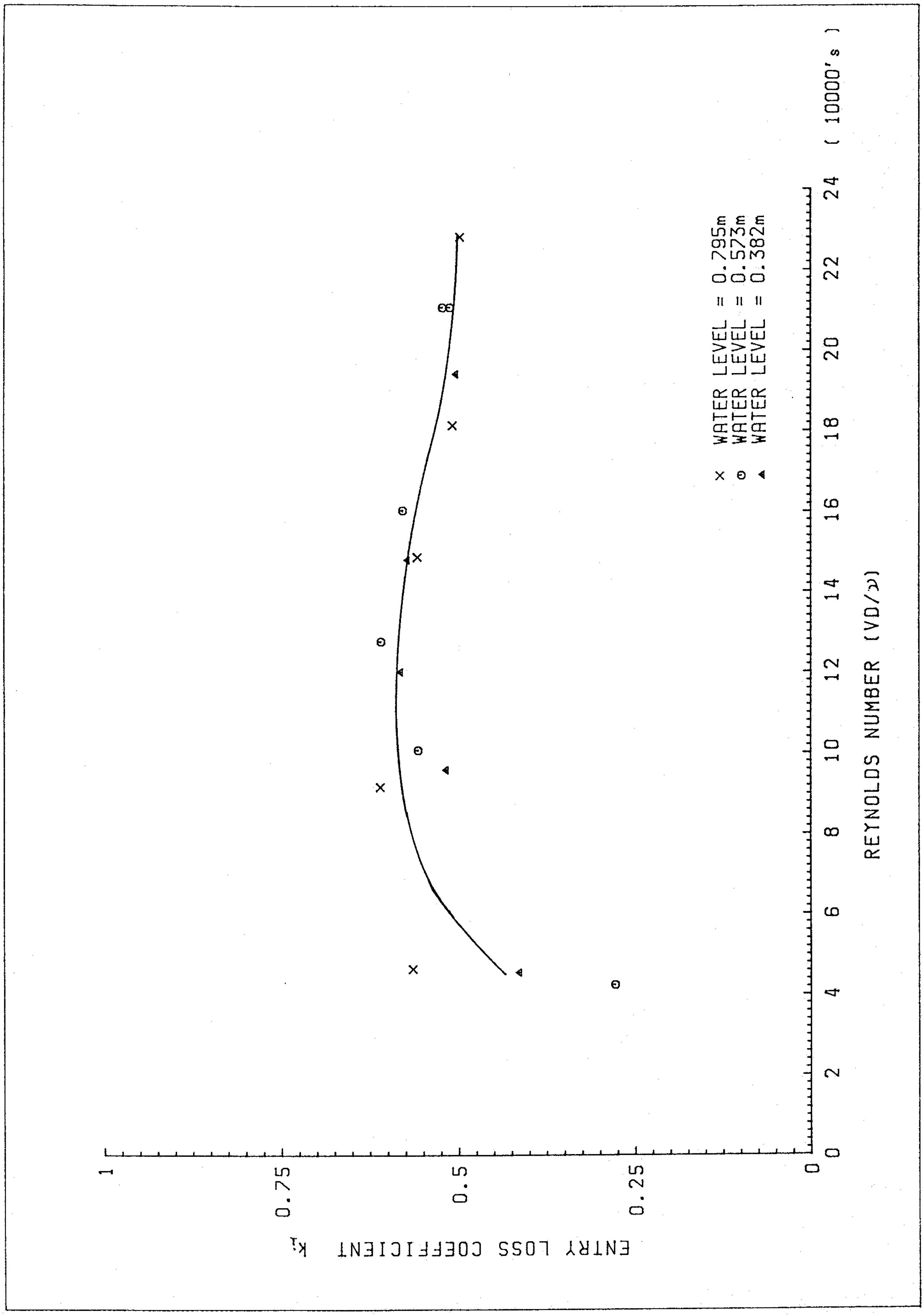

FIG 10b VARIATION OF ENTRY LOSS COEFFICIENT WITH REYNOLDS NUMBER FOR VERTICAL HEADWALL

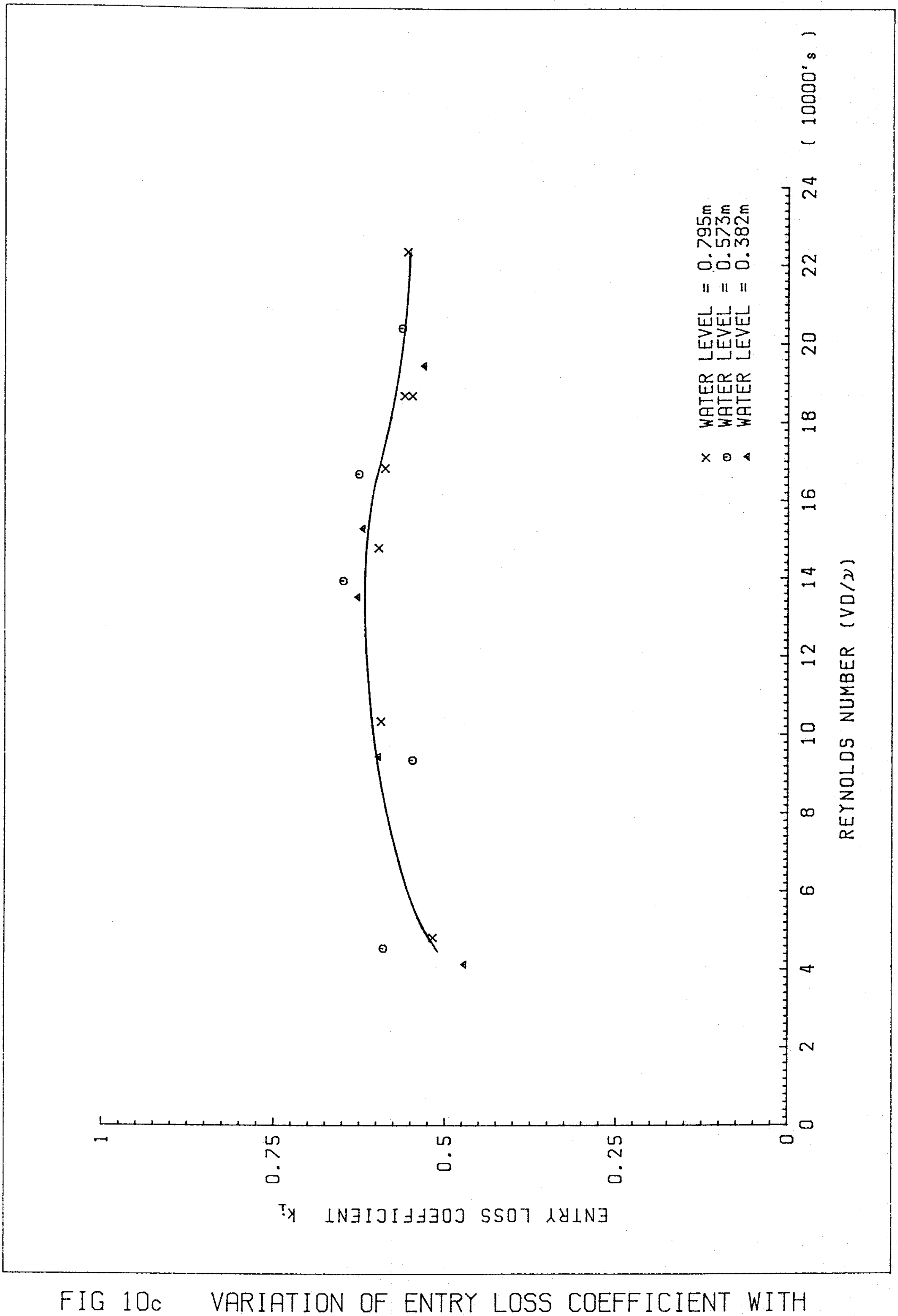

FIG 10c VARIATION OF ENTRY LOSS COEFFICIENT WITH REYNOLDS NUMBER FOR HOODED SCREEN

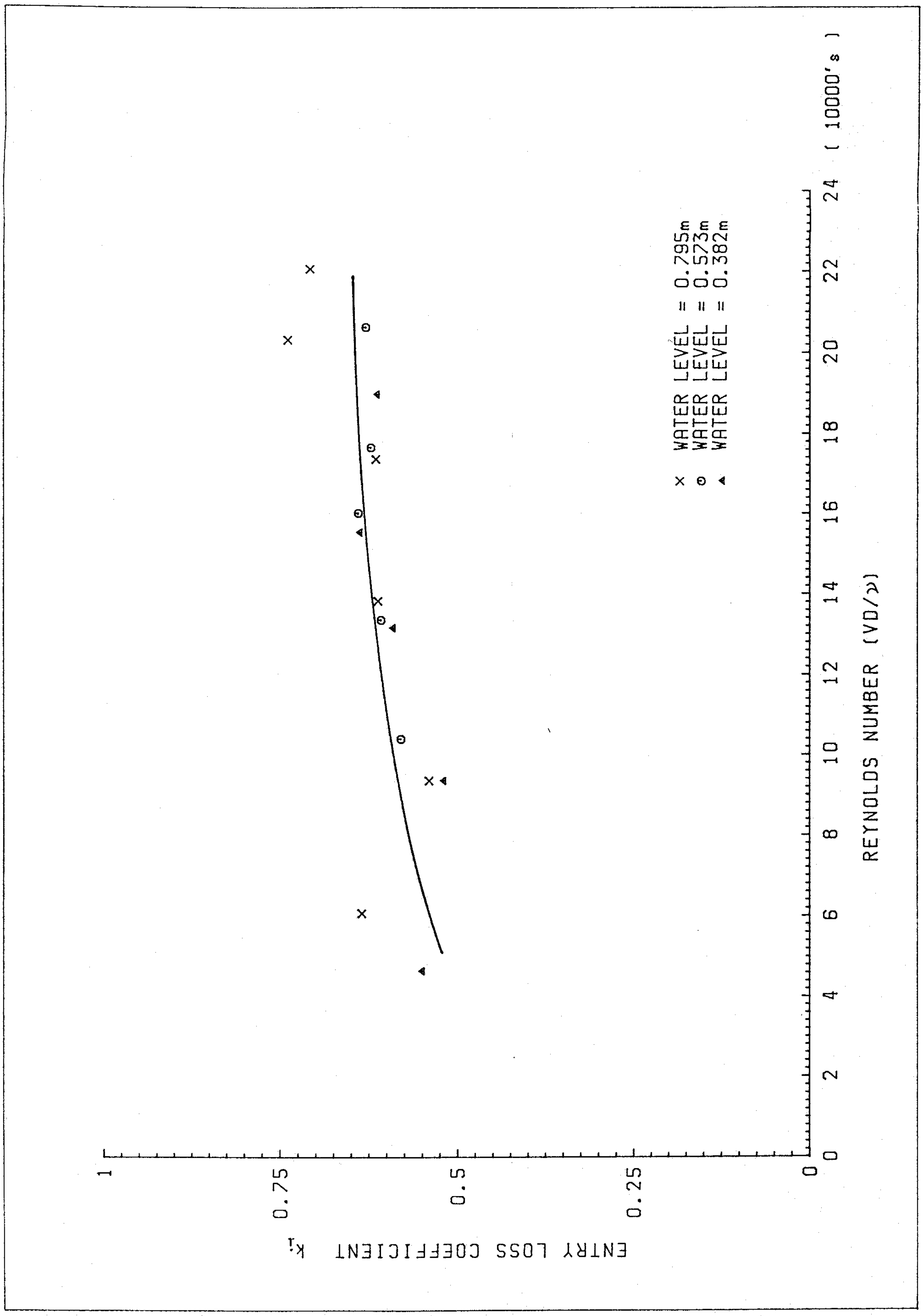

FIG 10d VARIATION OF ENTRY LOSS COEFFICIENT WITH REYNOLDS NUMBER FOR HEADWALL + HOODED SCREEN

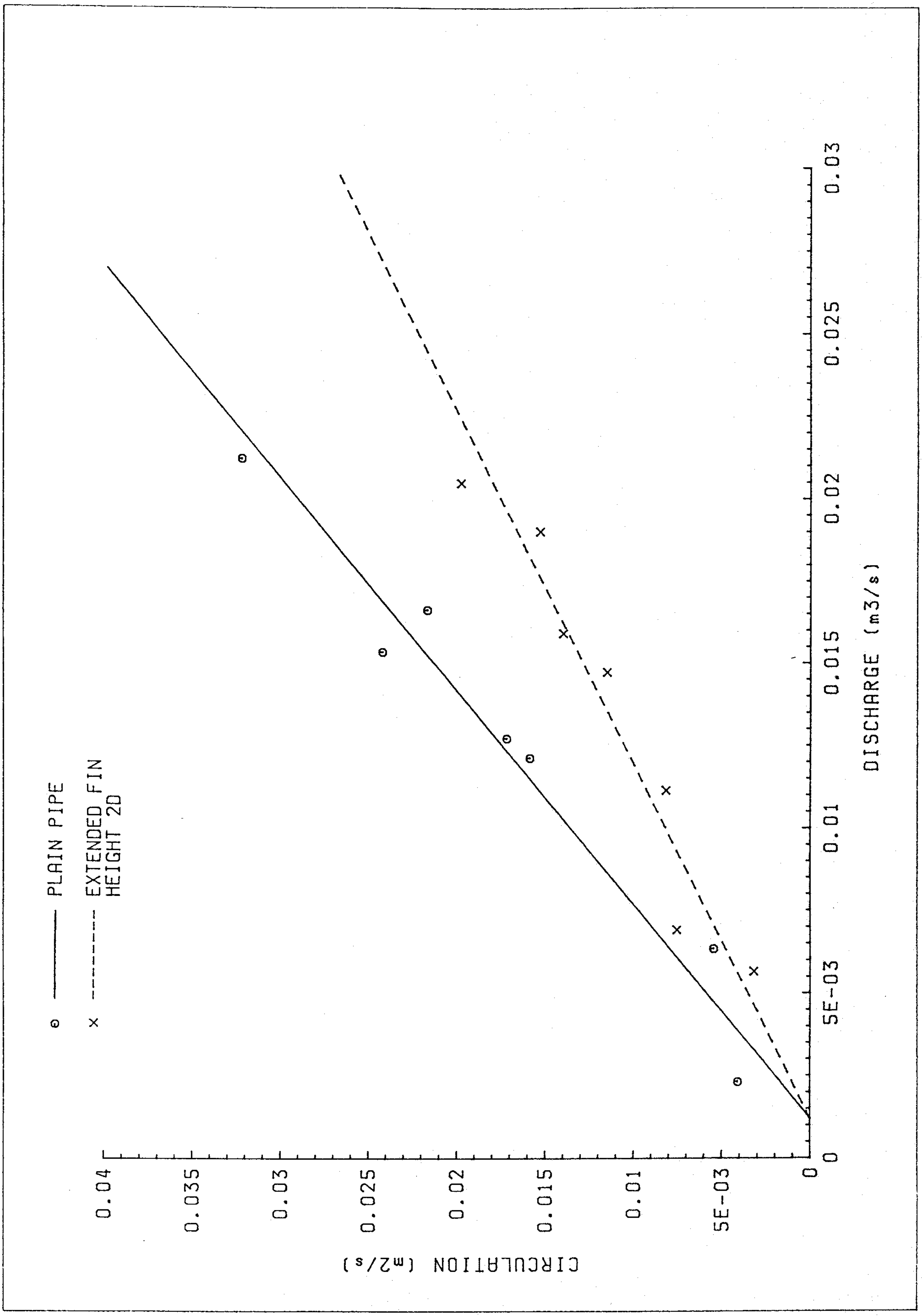

FIG 11a CIRCULATION STRENGTH V's DISCHARGE FOR PLAIN PIPE & EXTENDED FIN INHIBITOR , DEPTH = 0.382m

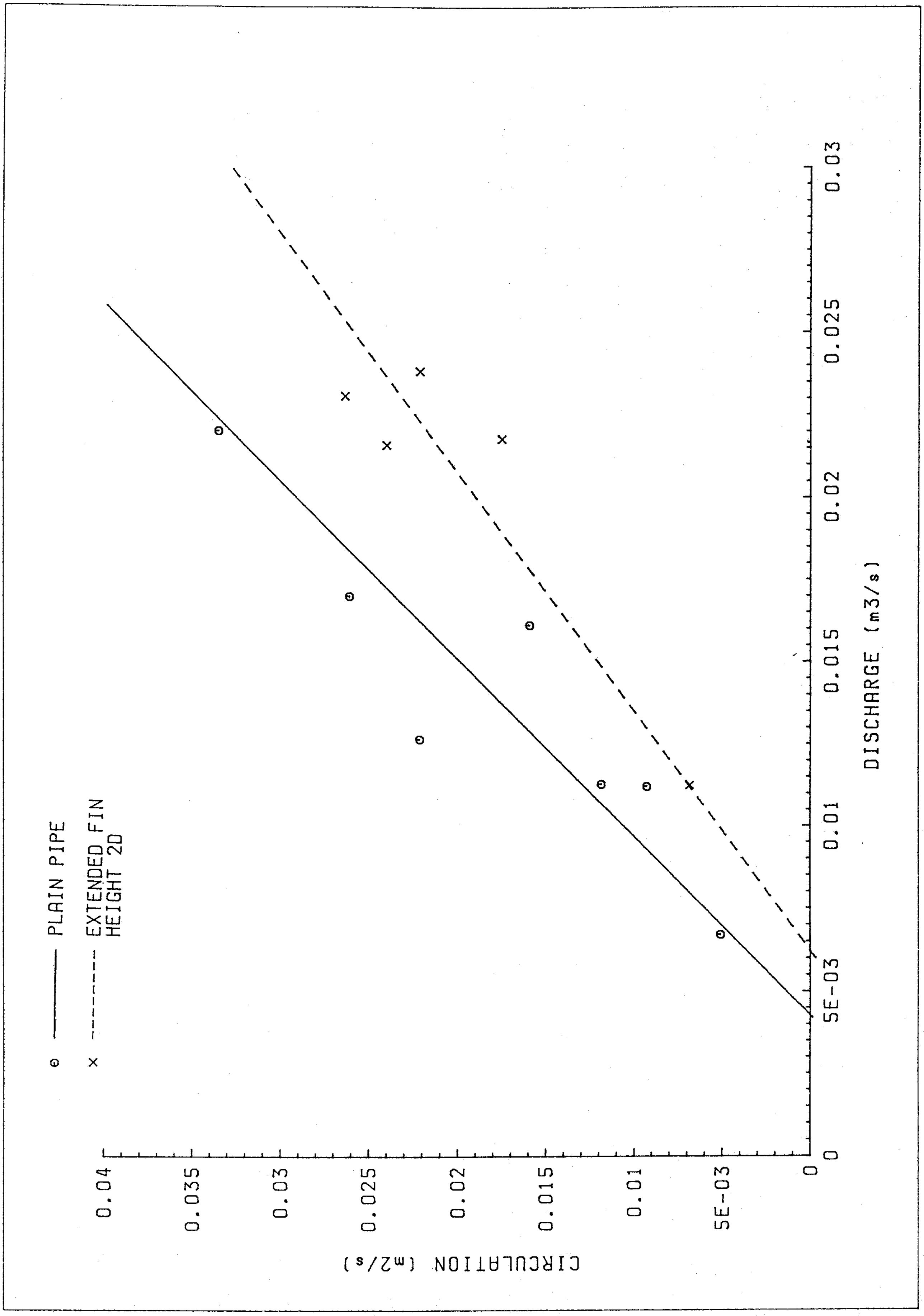

FIG 11b CIRCULATION STRENGTH V's DISCHARGE FOR PLAIN PIPE & EXTENDED FIN INHIBITOR , DEPTH = 0.573m

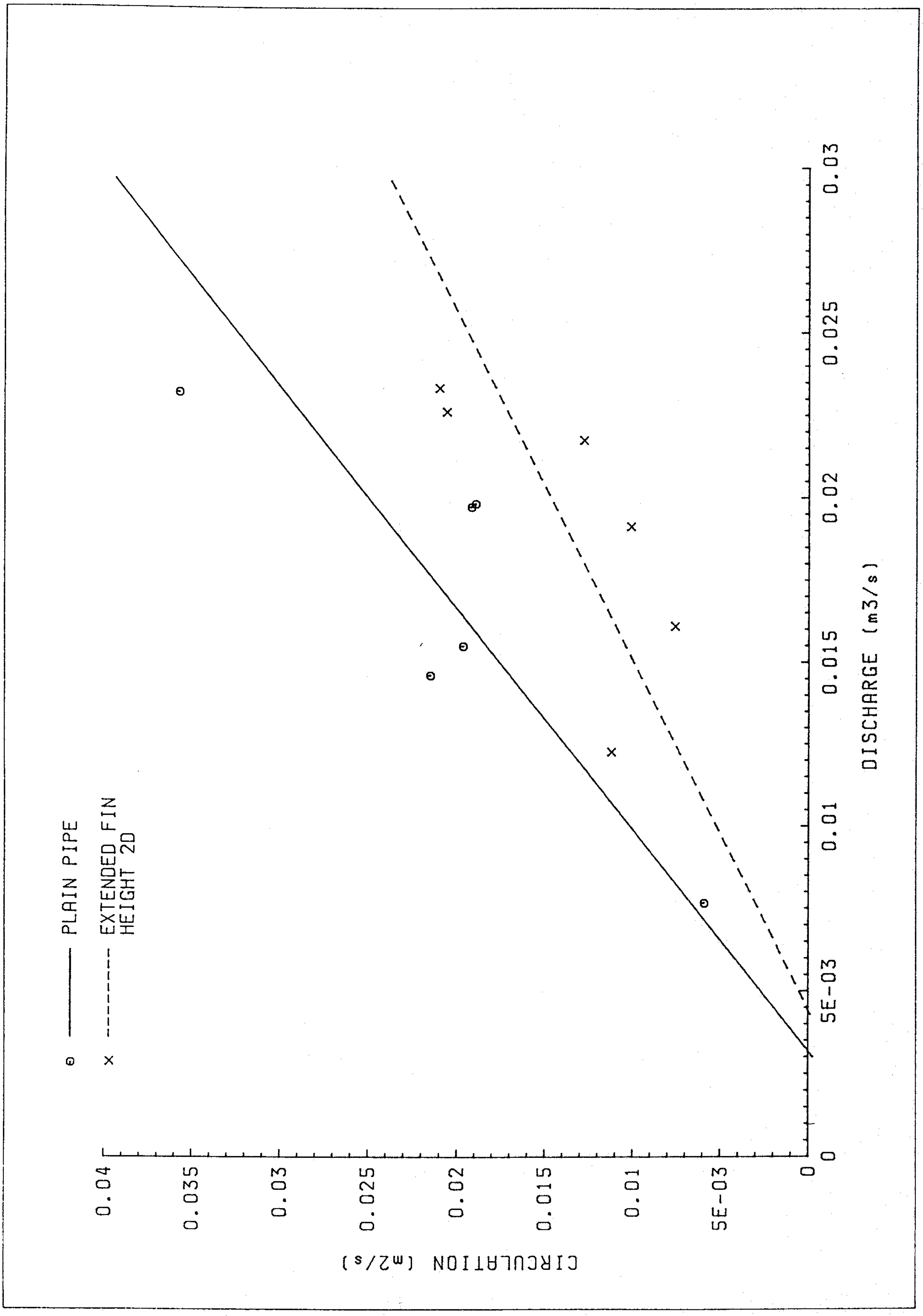

FIG 11c CIRCULATION STRENGTH V's DISCHARGE FOR PLAIN PIPE & EXTENDED FIN INHIBITOR , DEPTH = 0.795m

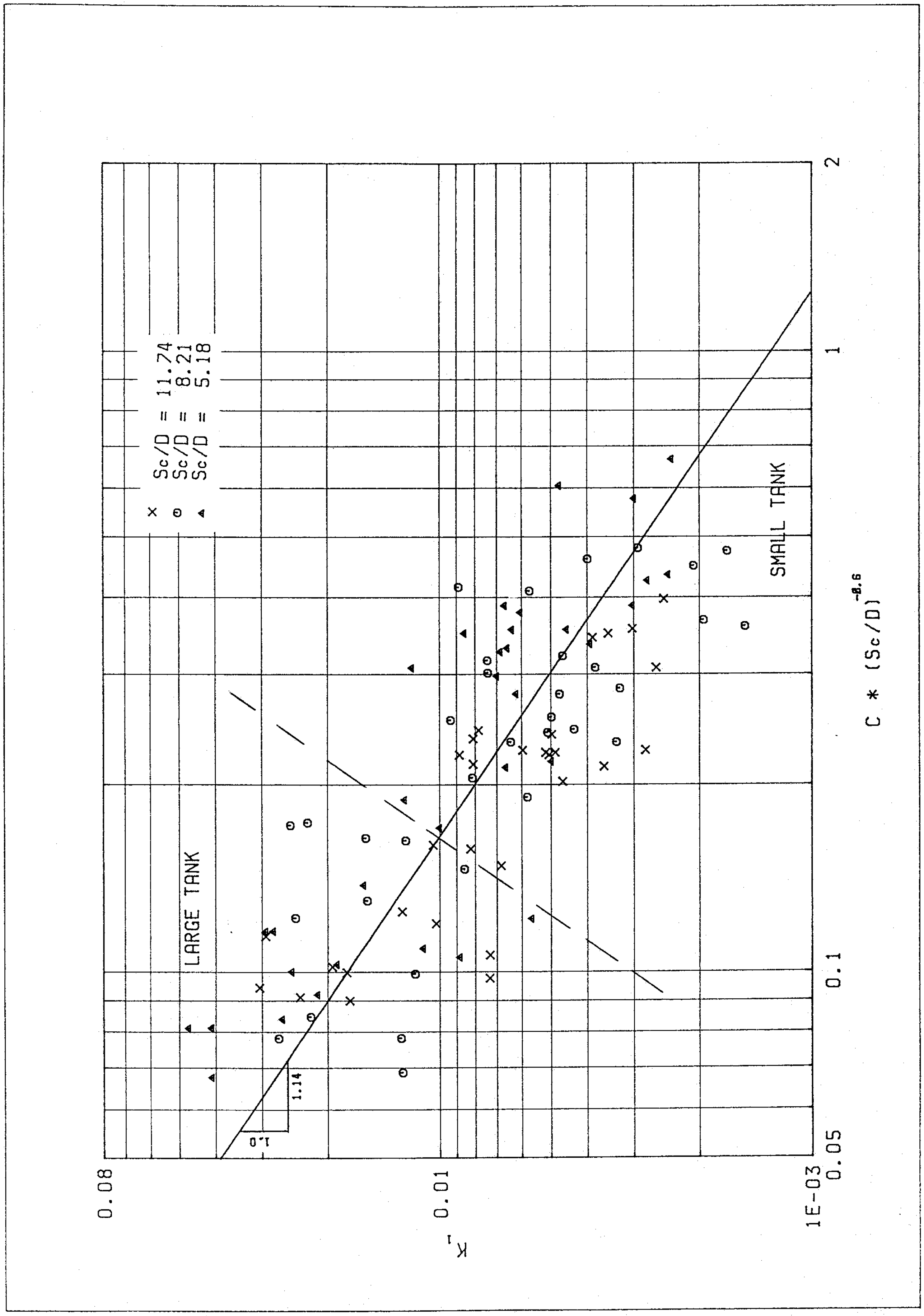

FIG 12a CORRELATION BETWEEN KOLF NUMBER AND DISCHARGE COEFFICIENT FOR DIMPLE

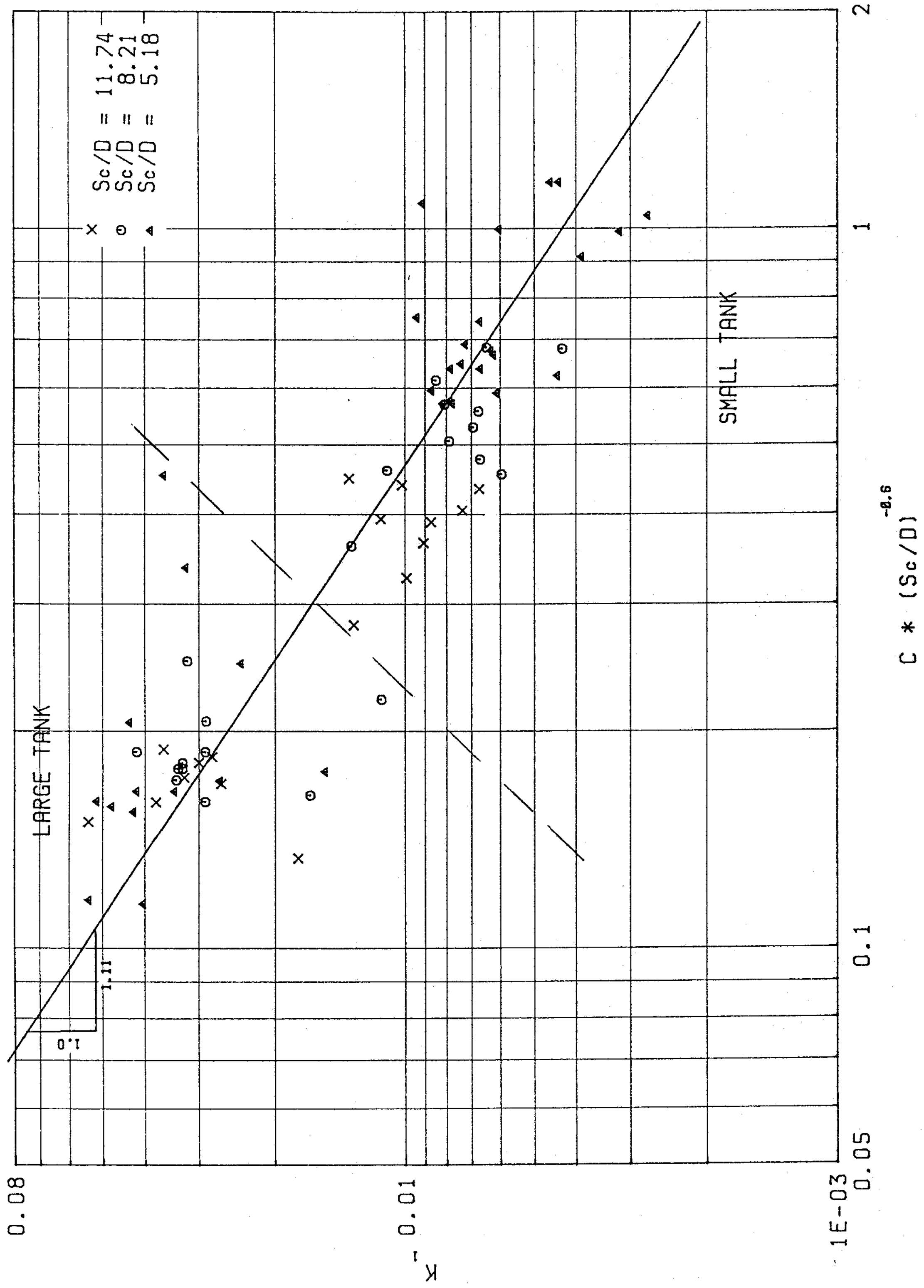

FIG 12b CORRELATION BETWEEN KOLF NUMBER AND DISCHARGE COEFFICIENT FOR MATERIAL DRAW-DOWN

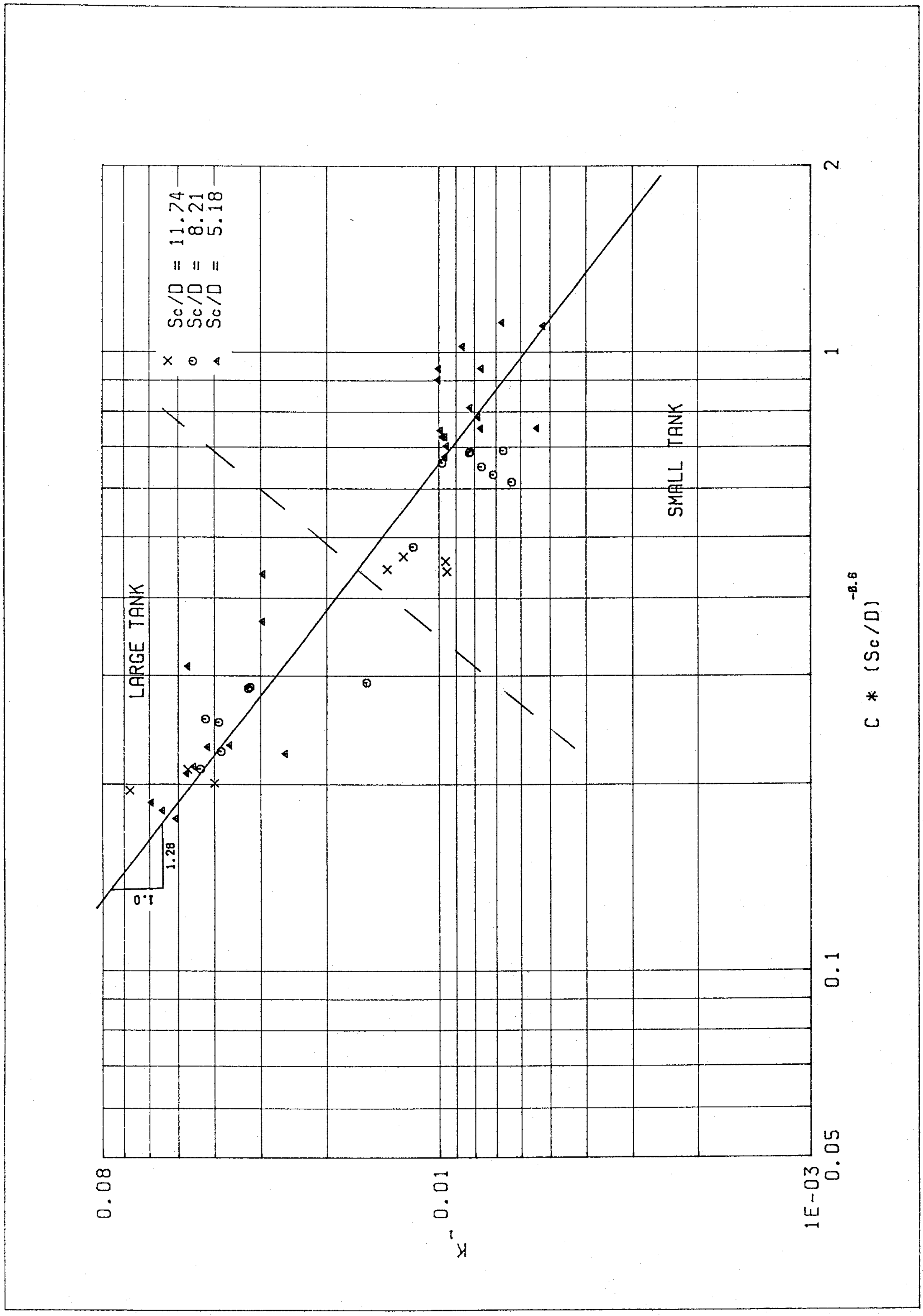

FIG 12c CORRELATION BETWEEN KOLF NUMBER AND DISCHARGE COEFFICIENT FOR AIR CORE

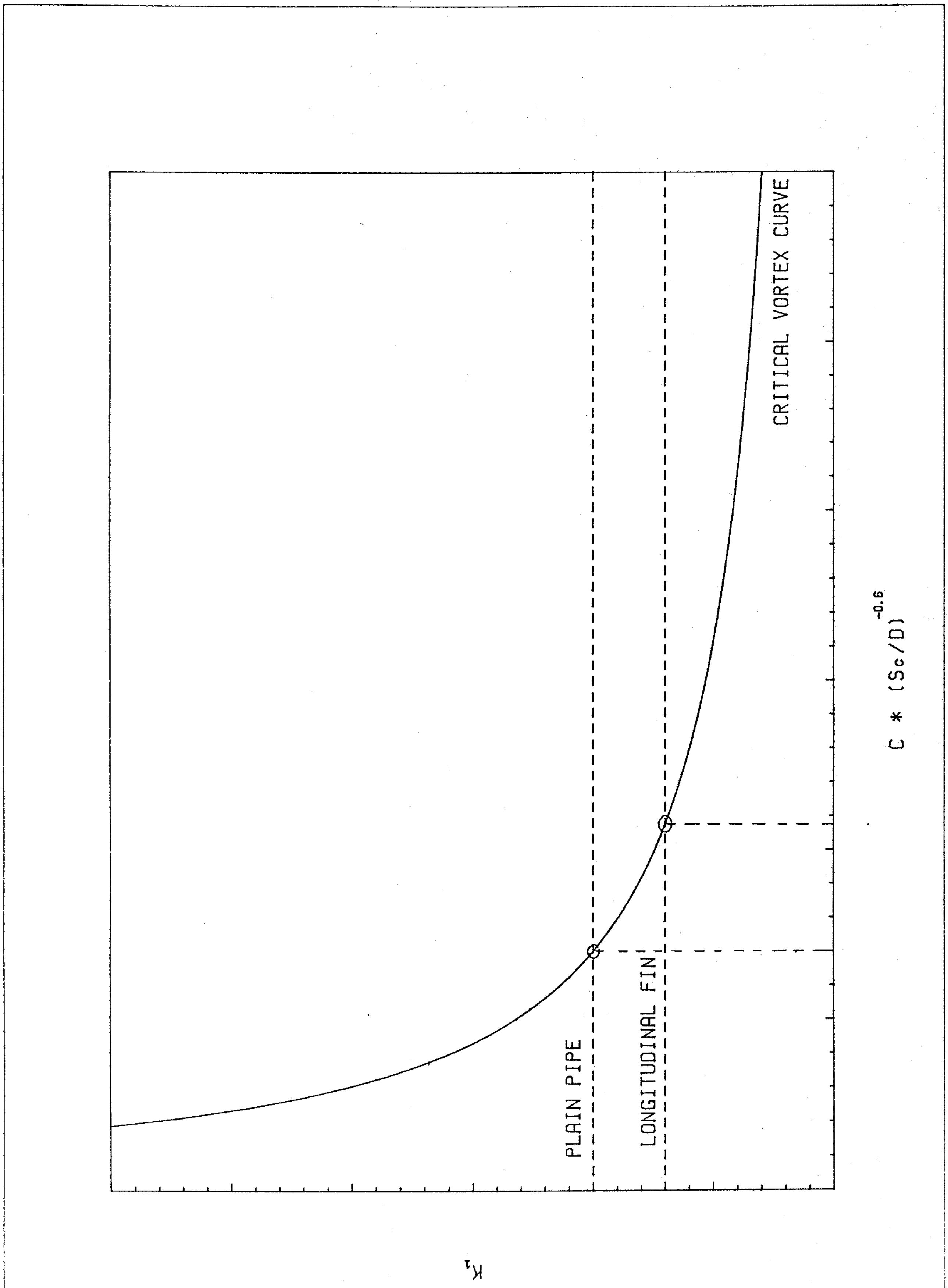

FIG 13 DIAGRAMMATIC REPRESENTATION OF VORTEX DEVELOPMENT

PLATES

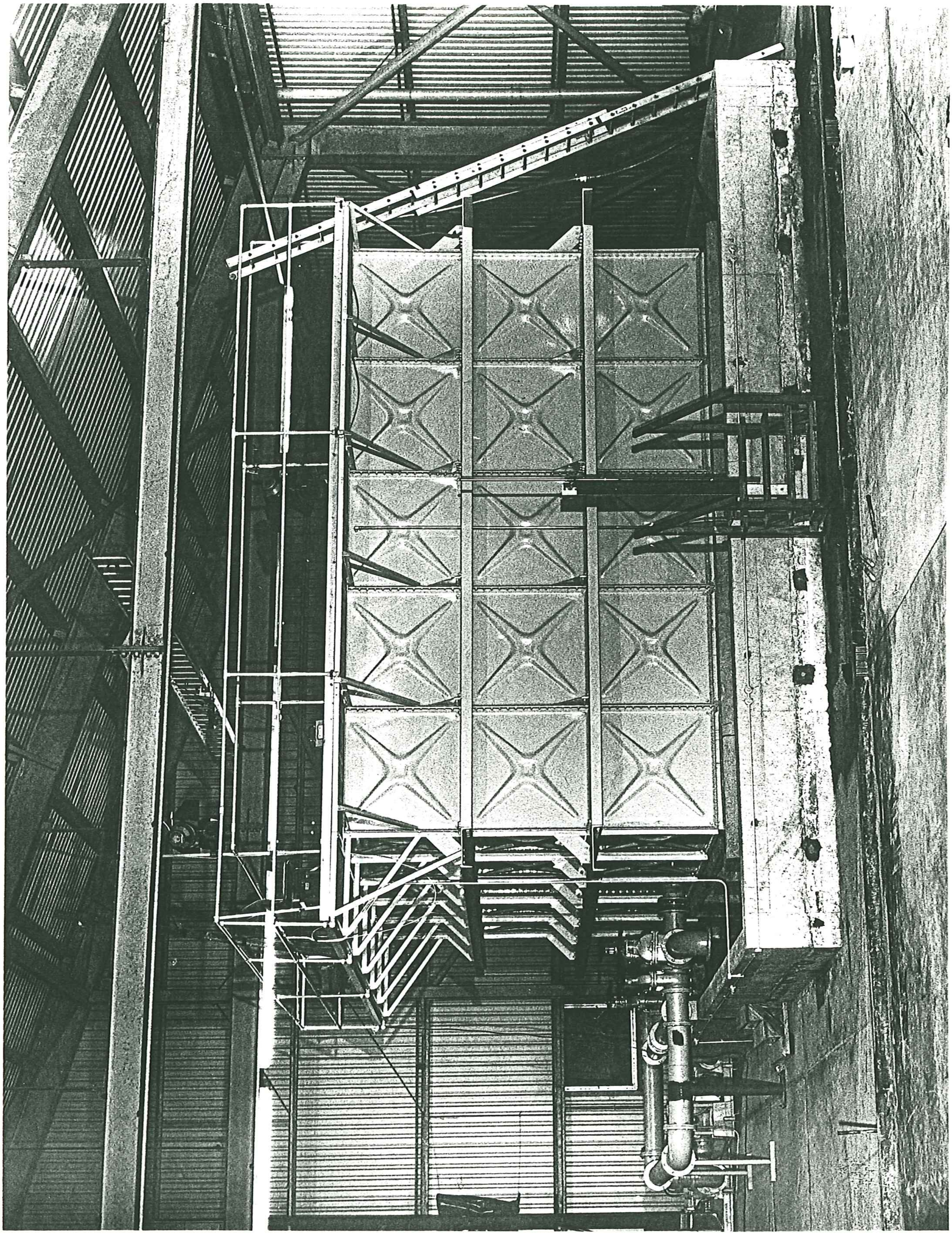

PLATE 1. Large Tank : external view

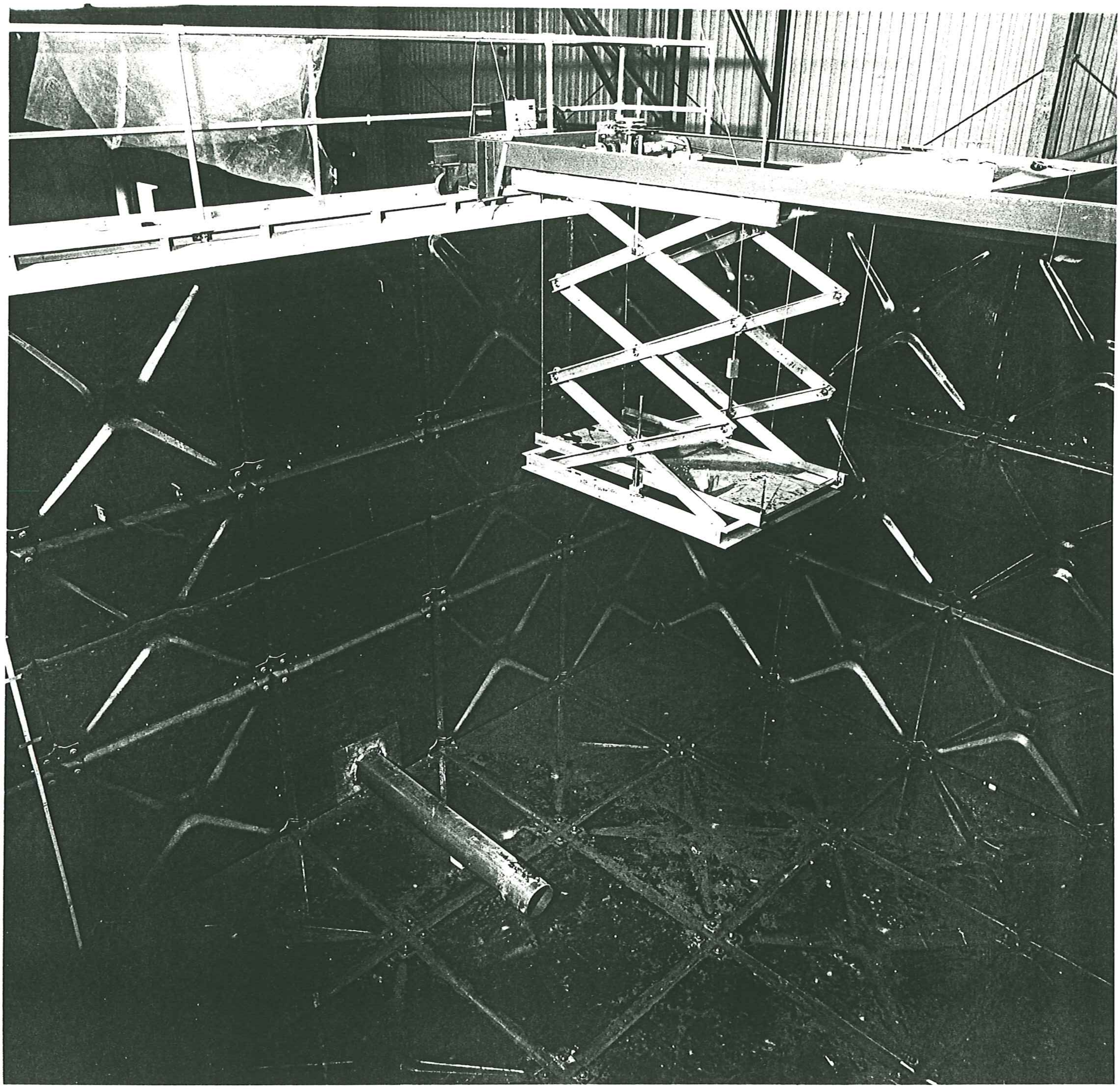

PLATE 2. Large Tank : internal view

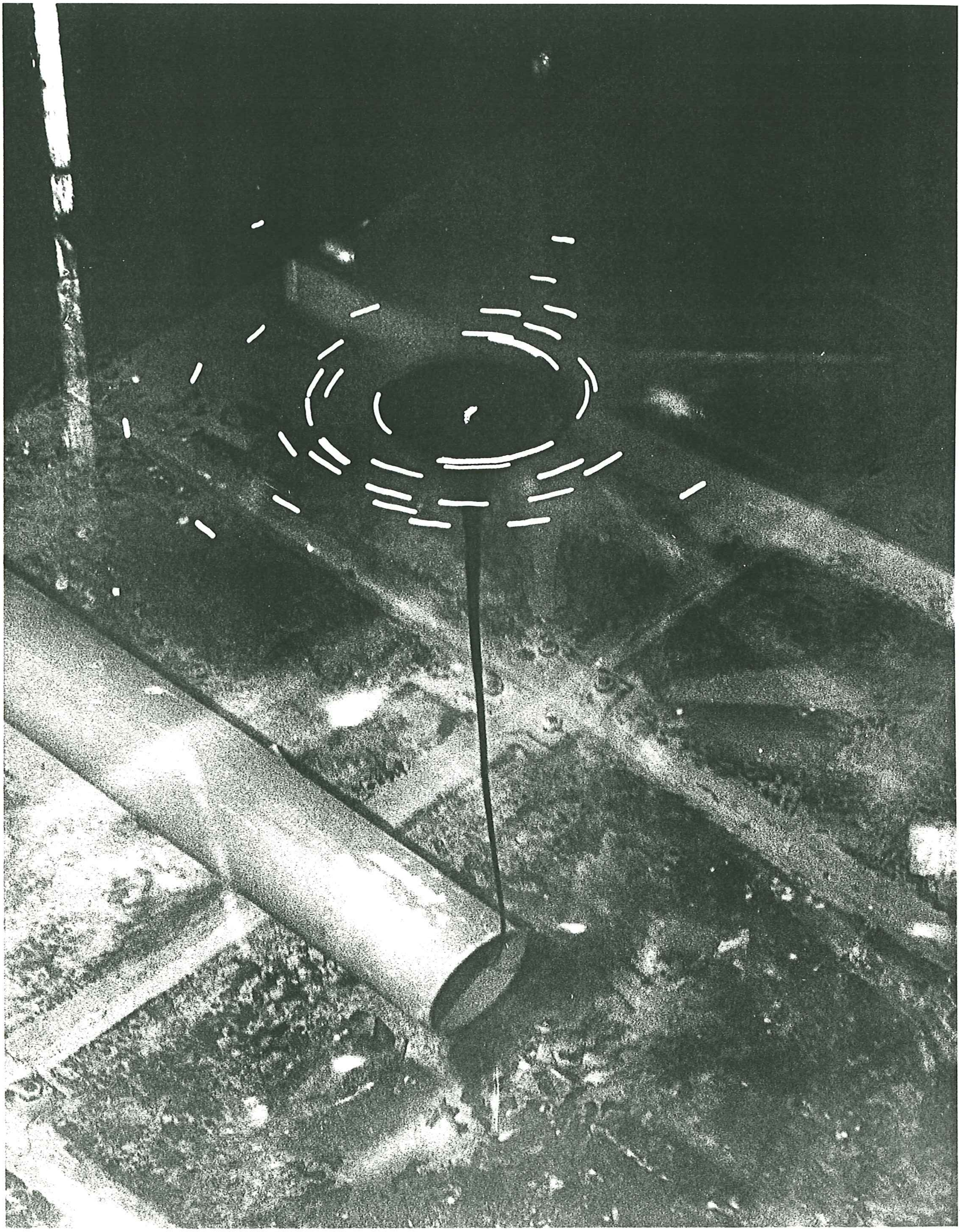

PLATE 3. Air-core vortex in Large Tank

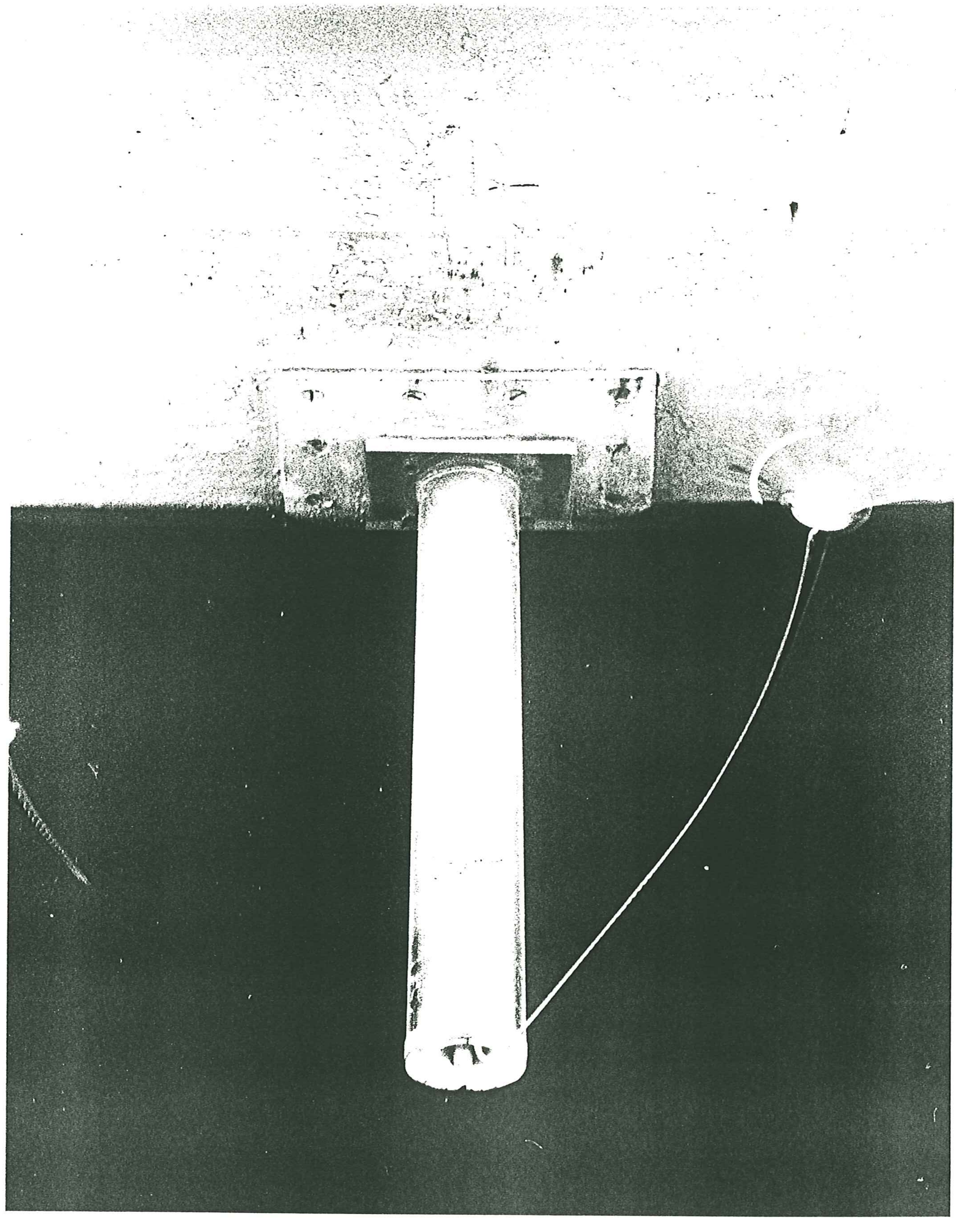

PLATE 4. Air-core vortex in Small Tank : from above

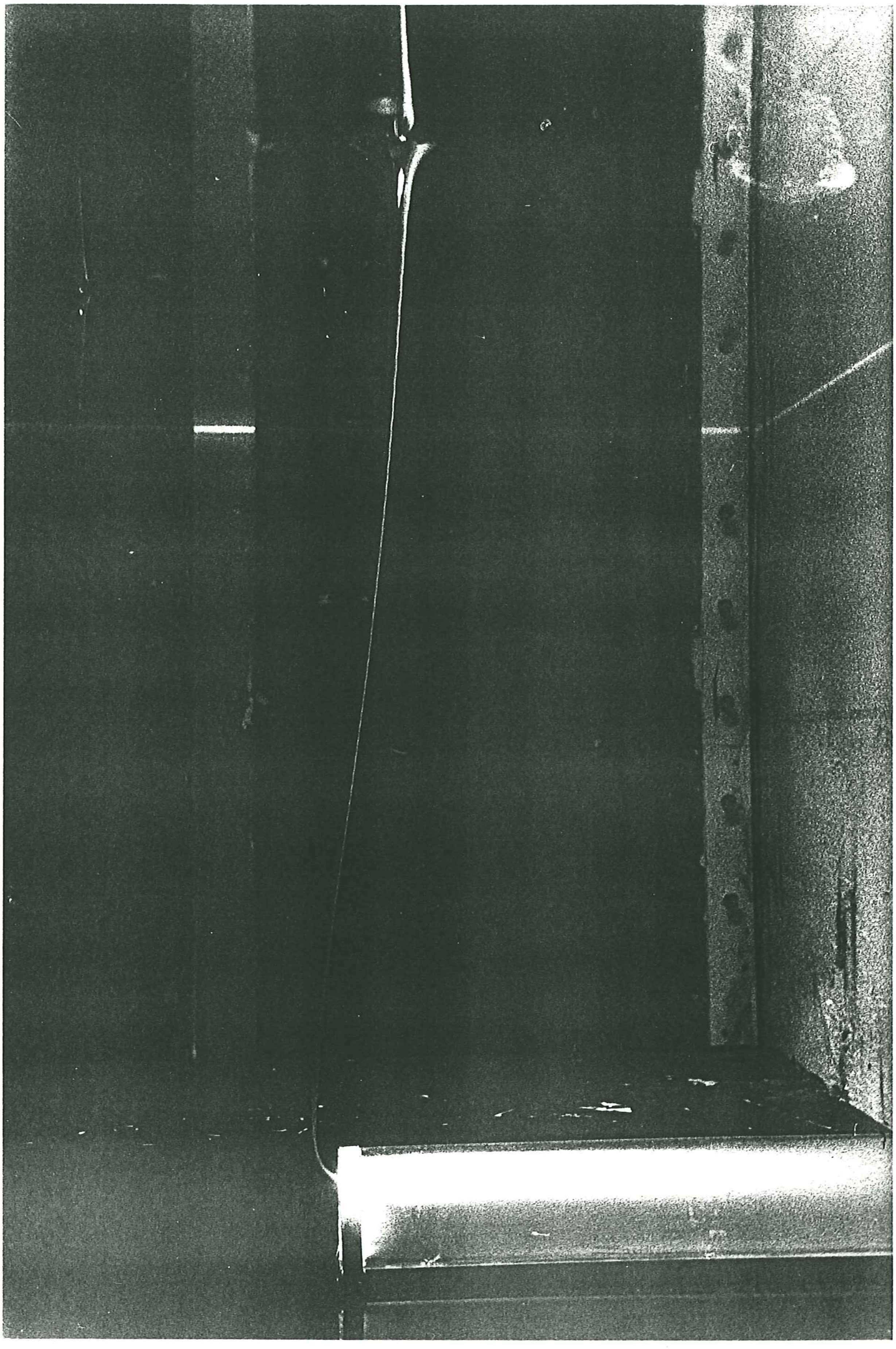

PLATE 5. Air-core vortex in Small Tank : from side

APPENDIX

APPENDIX A : GENERAL DESCRIPTION OF VORTEX ACTION

A.1 Dimensional analysis

Vortex motion is very complex and, in the absence of a satisfactory theoretical model, experimental results are usually analysed in terms of non-dimensional numbers. The primary variables to be considered are:

Q	Flow rate entering intake
S	Submergence depth to centreline of intake
D	Intake diameter (assumed here to be circular)
Γ	Circulation strength (see equations (3) or (4))
g	Acceleration due to gravity
μ	Viscosity of liquid
ρ	Density of liquid
σ	Surface tension of liquid

With eight variables and three independent dimensions, Buckingham's Pi theorem indicates that the motion should depend on five separate non-dimensional numbers. Previous researchers have combined the variables in many different ways, and this has tended to cause confusion and make comparisons difficult. In the absence of obvious reasons for favouring one grouping over another, it seems best to define them so that they refer specifically to ratios of forces, pressures or moments experienced by a fluid when subject to vortex motion. The following groupings are suggested:

(1) Froude number. Convergence of flow towards an intake lowers the static pressure (Bernoulli effect) and assists air to penetrate downwards through the vortex core. This inertial pressure drop should be compared with the hydrostatic

pressure due to the water depth. The ratio of inertial pressure/hydrostatic pressure is proportional to:

$$C = \frac{4Q}{\pi D^2 \ (2gS)^{\frac{1}{2}}} \qquad (A.1)$$

The numerical constants are introduced so that C is also equal to the conventional definition of discharge coefficient used for orifices discharging freely to atmosphere. This secondary definition is not relevant when the intake is connected to a pump or a long pipeline.

(2) Kolf number. Pressure in a vortex core is reduced both by the convergence of the flow (see (1)) and by its rotation. If the radius of the vortex core is r_o, then the ratio of rotational pressure drop/inertial pressure drop in the core is proportional to:

$$K = \frac{\Gamma r_o}{Q} \qquad (A.2)$$

The larger the value of K, the more important become the rotational effects.

(3) Submergence number. This is principally a geometric factor, and it seems reasonable to use the relative submergence ratio S/D. If the shape of the intake affects the length of the vortex core significantly, then this will be an additional factor (e.g horizontal intakes dictate longer vortex cores then vertical intakes).

(4) Reynolds number. Fluid viscosity acts to slow down the rotation of the fluid in the vortex core. The relevant factor here is the ratio

between the inertial torque due to the mass of the rotating fluid and the torque exerted by the viscous shear force. Considering unit length of the core, it can be simply shown that this ratio is proportional to

$$R_e = \frac{\Gamma}{\nu} \qquad \text{(A.3)}$$

The larger the value of R_e, the smaller is the effect of viscosity at the intake.

(5) Weber number. Surface tension can be significant only at an air-liquid interface. The effect should be most important when an air core is extending downwards towards an intake. At the tip of the core, surface tension will cause a pressure difference across the air-liquid interface due to its curvature. This pressure difference is proportional to σ/r_o and acts to make it harder for the air to penetrate downwards. It is therefore logical to compare this additional pressure with the hydrostatic pressure, and thus obtain the ratio:

$$W_e = \frac{\rho g r_o S}{\sigma} \qquad \text{(A.4)}$$

When this number is large, effects due to surface tension should not be significant.

It can be seen from the above analysis that two of the five parameters depend on the size of the vortex core, which is usually unknown or difficult to measure. If one wishes to obtain similarity between a prototype intake and a model, it seems reasonable to require that the size of the vortex core in relation to the size of the intake should be the same in both cases. On this basis, it becomes possible to replace r_o in equations (A.2) and (A.4) by D. However, this might not be correct if one were concerned with the conditions at which an air core just reaches an intake; in a prototype, it is likely that the core would be relatively smaller than it was in the model. Assuming that the substitution of D for r_o to be valid, the five independent non-dimensional parameters become:

$$C \, , \frac{\Gamma D}{Q} \, , \frac{S}{D} \, , \frac{\Gamma}{\nu} \, , \frac{\rho g \, DS}{\sigma}$$

A.2 Comparisons between previous studies

The critical flow conditions at which a continuous air core develops at an intake have been studied by several researchers, and it is instructive to express their results in terms of the parameters obtained in the previous section. Most researchers have considered or found the effects of surface tension to be negligible, so the Weber number will not be included in the analysis.

Daggett & Keulegan (1974) studied drain vortices in circular tanks using eight different sizes of orifice (D = 9.5mm to 102mm) and six fluids with various values of viscosity and surface tension. Analysis of data for the critical submergence S_c corresponding to air-core formation gave

$$\left(\frac{\Gamma D}{Q}\right)\left(\frac{S_c}{D}\right)^{-1} = 2.67 \times 10^{-2} \, , \text{ for } \left(\frac{Q}{D\nu}\right) > 2.14 \times 10^{4} \qquad \text{(A.5)}$$

$$\left(\frac{\Gamma}{\nu}\right)\left(\frac{S_c}{D}\right)^{-1} = 5.71 \times 10^2, \text{ for } \left(\frac{Q}{D\nu}\right) < 2.14 \times 10^4$$

(A.6)

Viscosity was found not to influence the vortex motion when $Q/D\nu$ exceeded 2.14×10^4.

Jain et al (1978) used a similar type of experimental arrangement to Daggett & Keulegan, but replaced the orifice by a vertical intake connected to a pump so that discharge could be varied independently of head. Tests were carried out in two circular tanks using six sizes of intake pipe and water-based solutions with various viscosities and surface tensions. Above a certain limit, the results were not affected by viscosity and were described by

$$\left(\frac{\Gamma D}{Q}\right)\left(\frac{S_c}{D}\right)^{-0.786} C^{1.190} = 1.095 \times 10^{-2} \quad \text{(A.7)}$$

Below this limit, viscous effects were found to be signficant, and the corresponding equation was:

$$\left(\frac{\Gamma}{\nu}\right)^{0.738}\left(\frac{\Gamma D}{Q}\right)^{0.262}\left(\frac{S_c}{D}\right)^{-1.155} C^{0.452} = 37.4 \quad \text{(A.8)}$$

The transition from viscous to non-viscous conditions occurs when

$$\left(\frac{Q}{D\nu}\right) > 6.14 \times 10^4 \, C \left(\frac{S_c}{D}\right)^{0.5} \quad \text{(A.9)}$$

Knauss (1987) analysed the data from these two studies together with results obtained by Anwar et al (1978) for horizontal intakes and by Anwar & Amphlett (1980) for vertically inverted intakes. Knauss concluded that in Jain et al's experiments the circulation strengths at the intake were approximately 2.2 times the assumed values (calculated from the angle of the inlet vanes around the periphery of each test tank). Making this adjustment and concentrating on the non-viscous results, Knauss developed the following equation

$$\left(\frac{\Gamma D}{Q}\right) \left(\frac{S_c}{D}\right)^{-0.5} C = \Omega \qquad (A.10)$$

where $\Omega = 0.0535$ for a vertical intake, $\Omega = 0.0628$ for a horizontal intake and $\Omega = 0.0752$ for a vertically-inverted intake (e.g. the suction pipe of a pump).

Comparison of equations (A.5) to (A.10) shows some clear similarities and trends. In the case of Daggett & Keulegan's study, the outlets discharged freely under gravity so the discharge coefficient C would have been approximately constant and equal to about 0.65. For non-viscous conditions, Equations (A.5), (A.7) and (A.10) suggest that the exponent of C is about 1.0 and that of (S_c/D) is in the range -0.5 to -1.0. Daggett & Keulegan's Equation (A.6) indicates that, under viscous conditions, the Reynolds number term (Γ/ν) becomes dominant and the Kolf number $(\Gamma D/Q)$ loses its significance. Jain et al's Equation (A.8) suggests that their data were in a transition zone where both parameters were relevant, although the viscous term (Γ/ν) was the more important. In both cases, the exponent of (S_c/D) was about 1.0.

A.3 Unified formula for vortex inception

The comparisons described above point to the possibility of developing a unified formula for vortex inception that can describe the transition from fully viscous to non-viscous conditions - a separate relationship would apply for each stage of vortex formation (eg surface dimple, material draw-down, air core). Such a formula would be useful when evaluating scale effects associated with model tests of intakes. Unfortunately, no general theory is yet available to guide the choice of equation, so it is necessary to rely on the evidence of the results described in A.2, while recognising that they represent approximate best fits to data with appreciable scatter.

Various forms of equation have been considered, and the following is proposed as an initial model for further study.

$$\frac{(S_c/D)^{-n}\ C^{1.2}}{(Q/\Gamma D) + \alpha\ C^m\ (\nu/\Gamma)} = \beta \tag{A.11}$$

where α, β, m and n are constants to be determined. The transition between viscous and non-viscous conditions in Equation (A.11) is accomplished in a similar way to that in the Colebrook-White resistance formula. Comparison with the previous equations suggests that m might have a value of approximately 1.0 and n might be in the range 0.5 to 1.0. The values of circulation strength, discharge and submergence obtained in the present study have been compared with the following version of Equation (A.11) on the assumption that all the data for a given vortex strength should be governed by the same relationship irrespective of the particular design of inhibitor.

$$K_1 = \frac{(\Gamma D/Q)}{1 + \alpha C (\nu D/Q)} = \beta \left(C \left(\frac{S_c}{D}\right)^{-0.6} \right)^{-1.} \quad (A.12)$$

Figures 12 a,b,c show the modified Kolf number K_1 (with $\alpha = 1.0 \times 1.0^6$) plotted against $C (S_c/D)^{-0.6}$ for the three vortex strengths which were studied: dimple, material draw-down and air core. The dimple data show a considerable amount of scatter, but this may reflect the difficulty of identfying and measuring very weak vortices. The results for material draw-down and air-core formation appear to fit Equation (A.12) reasonably well, and show that the modified Kolf number is successful at correlating data from the large and small test tanks. Further testing of equation (A.12) is necessary using data from other studies.

A.4 References

ANWAR H.O., WELLER J.A. & AMPHLETT M.B. (1978). Similarity of free-vortex at horizontal intake. Jnl Hydr Res, Vol 16, No 2, pp 95 - 105.

ANWAR H.O. & AMPHLETT M.B. (1980). Vortices at vertically inverted intake. Jnl Hydr Res, Vol 18, No.2, pp 123-124.

DAGGETT L.L. & KEULEGAN G.H. (1974). Similitude in free-surface vortex formations. Jnl Hydr Div, Amer Soc Civ Engrs, Vol 100, No.11, pp 1565-1581.

JAIN A.K, RAJU K.G.R. & GARDE R.J. (1978). Air entrainment in radial flow towards intakes. Jnl Hydr Div, Amer Soc Civ Engrs, Vol 104, No.9, pp 1323-1329.

KNAUSS J.(1987). Swirling flow problems at intakes. Hydraulic Structures Design Manual 1.A.A. Balkema, Rotterdam.(See Chapter 4).